Materials Horizons

ROYAL SOCIETY OF CHEMISTRY

REVIEW

View Article Online
View Journal | View Issue

Cite this: *Mater. Horiz.*, 2021, **8**, 661

Highly selective gas sensing enabled by filters

Jan van den Broek, Ines C. Weber, Andreas T. Güntner and Sotiris E. Pratsinis *

Received 8th September 2020,
Accepted 12th November 2020

DOI: 10.1039/d0mh01453b

rsc.li/materials-horizons

Portable and inexpensive gas sensors are essential for the next generation of non-invasive medical diagnostics, smart air quality monitoring & control, human search & rescue and food quality assessment to name a few of their immediate applications. Therein, analyte selectivity in complex gas mixtures like breath or indoor air remains the major challenge. Filters are an effective and versatile, though often unrecognized, route to overcome selectivity issues by exploiting additional properties of target analytes (*e.g.*, molecular size and surface affinity) besides reactivity with the sensing material. This review provides a tutorial for the material engineering of sorption, size-selective and catalytic filters. Of specific interest are high surface area sorbents (*e.g.*, activated carbon, silica gels and porous polymers) with tunable properties, microporous materials (*e.g.*, zeolites and metal–organic frameworks) and heterogeneous catalysts, respectively. Emphasis is placed on material design for targeted gas separation, portable device integration and performance. Finally, research frontiers and opportunities for low-cost gas sensing systems in emerging applications are highlighted.

1. Introduction

Gas sensors allow modern electronic devices to smell their environment. By utilizing portable and inexpensive sensors, a multitude of promising applications[1] can be realized (Fig. 1): smart air quality control (indoor[2] and outdoor[3]) with distributed, interconnected or drone-borne sensors that communicate wirelessly chemical data in real-time to map toxic pollutants (*e.g.*, formaldehyde,[4] NO_x[5] or CFC-11[6]); food quality assessment[7] to monitor the production and distribution from plant growth (*e.g.*, plant hormone ethylene[8]), regulate processing (*e.g.*, acetic acid for aroma development in coffee[9]) and detect spoiling (*e.g.*, ammonia for meat[10]) to minimize waste; non-invasive medical diagnostics by breath analysis[11] to detect

Particle Technology Laboratory, Institute of Energy & Process Engineering, Department of Mechanical and Process Engineering, ETH Zurich, CH-8092 Zurich, Switzerland. E-mail: sotiris.pratsinis@ptl.mavt.ethz.ch

Jan van den Broek

Jan van den Broek received his MSc (2016) in material science from ETH Zürich, Switzerland where he is now a PhD candidate in mechanical and process engineering. He develops highly selective gas sensing systems by combining chemical sensors with sorption filters. For this he received the best poster award in Exposure Measurement Methods and Techniques during the 2019 Annual Meeting of the European Aerosol Conference in Gothenburg, Sweden that was attended by over 1000 registered participants. Today he focuses on the integration of sensors into handheld devices and realistic testing for breath analysis, air pollution monitoring and food quality assessment.

Ines C. Weber

Ines C. Weber received her BSc (2016) and MSc (2018) in material science from the Swiss Federal Institute of Technology (ETH Zürich). Currently, she is a PhD candidate at the Particle Technology Laboratory in the Mechanical and Process Engineering Department at ETH Zürich. Her research centers around highly selective nanostructured gas sensors enabled by reactive filter design. A particular focus is their use for breath analysis in medical and lifestyle applications, as well as indoor and outdoor air quality monitoring, in close collaboration with the Department of Chemistry at ETH Zürich and the University Hospital Zürich.

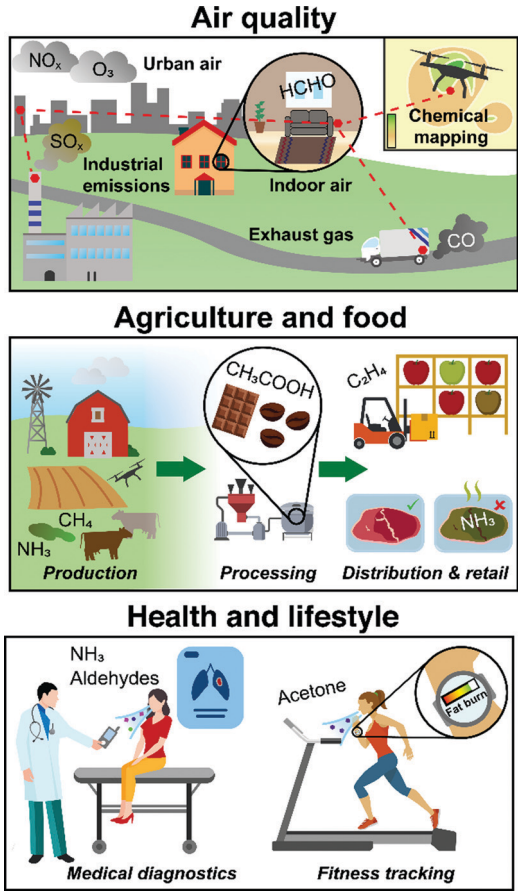

Fig. 1 Compact and low-cost gas sensors in air quality monitoring, agriculture & food quality assessment and health & lifestyle applications.

diseases (*e.g.*, cancer[12] or diabetes[13]) and monitor their progression, or personalized tracking of physiological data (*e.g.*, dieting[14] or exercise[15]); and in human search and rescue[16] to assist first responders with robots capable to detect the unique human chemical signature[17] similar to dogs (*e.g.*, after earthquakes or avalanches[18]), just to highlight some.

For integration into electronic devices, gas sensors need to be compact, inexpensive and simple-in-use. Most importantly, they need to detect selectively volatile organic compounds (VOCs) and gases at low ppb to ppm (parts-per-billion/million by volume) concentrations in mixtures without interference over hundreds of others (*e.g.*, >800 in breath[19] or >250 in indoor air[20]). State-of-the-art gas sensors (*e.g.*, chemoresistive[21] or optical[22]) provide this sensitivity by making use of nanomaterials having high specific surface area (*e.g.*, 5 ppb acetone at 90% relative humidity (RH) by leached nanostructured Pd/SnO_2[23] or sub-ppb detection of Cl_2 by nanoparticle-based liquid crystal sensors[24]).

Most challenging, however, is selectivity, which can be tuned to some extent by material composition of single sensors including metastable phases,[25] solid solutions,[26] mixed oxides[27] or heterostructures with unique morphology (*e.g.*, hollow nanofibers[28] or ordered macroporous oxides[29]). For example, the epsilon phase of WO_3 (*i.e.*, ε-WO_3) stabilized by Cr-doping showed some acetone selectivity (>6) to ethanol, methanol NO_x, NH_3 and CO.[25] Also, $In_4Sn_3O_{12}$ reacts selectively to formaldehyde,[30] Ti/ZnO to isoprene,[31] Si/α-MoO_3 to ammonia,[32] or Ag/$LaFeO_3$ to methanol.[33] However, such selectivities are typically only moderate, apart rare exceptions exploiting unique analyte-sensor interactions (*e.g.*, CuBr for ammonia[34] or WO_3 for NO_2[35]). This is often not sufficient in applications where interferant concentrations may be orders of magnitude higher than the target analyte (*e.g.*, <8 ppb carcinogenic[36] formaldehyde in indoor air with ~1000 ppb CO background[37]).

To discriminate between analytes in gas mixtures, different sensors can also be combined to arrays (also called electronic

Andreas T. Güntner

Dr Andreas Güntner received his PhD (2016) in mechanical and process engineering from ETH Zürich where he is currently a lecturer and research group leader. His research aims to advance the understanding of micro & nanoscaled materials at the interface between physics, chemistry and medicine. The development of new sensing technologies in healthcare and environmental applications is a particular emphasis. He is double recipient of the ETH Medal, the Excellence Award for Product Design and Engineering from the European Federation of Chemical Engineering and the Gesellschaft für Aerosolforschung (GAeF) PhD Award by the Association for Aerosol Research, among other recognitions.

Sotiris E. Pratsinis

Professor S. E. Pratsinis teaches Mass Transfer and Micro-Nano-Particle Technology at ETH Zürich. He has graduated 43 PhDs, now at leading positions in industry and academia worldwide. Currently he advises four PhDs and four post-docs. He has published 400+ refereed articles, filed 20+ patents that are licensed to industry and have contributed to creation of four spinoffs. His research on multiscale particle dynamics pioneered flame aerosol synthesis of nanomaterials with closely controlled characteristics. This contributed decisively to identifying the origins of nanosilver toxicity, led to novel heterogeneous catalysts and, for the first time, flame-made gas sensors, nutritional supplements, dental and theranostic materials.

noses or E-noses), overcoming selectivity limitations of single sensors.[38] Reviews on material design,[39] data processing algorithms[40] and applications (*e.g.*, food quality and safety monitoring,[41] or breath analysis[42]) of sensor arrays address their potential. Generally, arrays process different sensor signals by statistical models to classify different odors. A variety of algorithms is used based on descriptive[43] (*e.g.*, principle component analysis, hierarchical cluster analysis) and predictive methods[44] (*e.g.*, artificial neural networks), often requiring a large set of data to "train" the models. Typically, arrays do not detect and discriminate specific analytes, but rather distinguish and classify analyte patterns (*i.e.*, odors). For instance, a sensor array might differentiate lung cancer patients from healthy subjects[45] or distinguish different quality grades of Indian black tea.[46] Thereby, often broadly sensitive sensors are used, making the array susceptible to overfitting and bogus correlations from confounders.[47] To discriminate multiple analytes and detect them with high accuracy in gas mixtures, distinctly selective sensors, ideally with orthogonal features,[48] are most desirable for inclusion into arrays.

Filters represent a third approach to enhance the selectivity of gas sensors. They were first discussed in a review about selectivity in semiconductor gas sensors in 1987.[49] Since then, filters were treated only as a side aspect in many books and reviews of gas sensors in general,[50] gas sensor types (*e.g.*, metal-oxide,[51] arrays,[52] zeolite,[53] metal–organic frameworks,[54] mesoporous materials,[55] combustible[56]) and applications (*e.g.*, environment, health and safety,[57] automotive,[58] explosives,[59] pollution,[60] indoor air quality,[2] health monitoring and disease diagnostic[61]). Placed either in front (*e.g.*, packed beds) or directly on top (*e.g.*, overlayers) of sensors, filters alter the composition and/or concentration of analytes in gas mixtures before reaching the sensor. In the ideal case, the target analyte is not affected while interferants are removed, resulting in high selectivity (>1000) even with non-selective sensors.[62] Already in 1980, a packed bed of zeolite 3A was tested to filter H_2S to selectively detect H_2 by a commercial SnO_2 sensor (Taguchi, Figaro).[62] Also, SiO_2-covered SnO_2 sensors eliminated interference by CO, CH_4, ethanol and isobutane for selective H_2 detection,[63] charcoal and carbon cloth were used to protect CH_4 sensors from poisoning by siloxanes,[64] and zeolite 5A filters blocked H_2S and ethylene for selective CO detection.[65] Today, filters are well-established in most industrial sensors (*e.g.*, CO[66] and CH_4[67] alarm sensors), however, their immense potential remains rather unexplored.

Only recently, filters were used to overcome selectivity issues of sensors for other, so far inaccessible, applications such as revealing methanol-adulterated liquors by separating methanol from ethanol in a packed bed sorption filter,[68] detecting H_2 leaks to fulfil, for the first time, stringent national standards by a polymer membrane on top of a plasmonic sensor,[69] and monitoring body fat burn from breath acetone by combusting interferants on a Pt/Al_2O_3 filter[70] preceding a Si/WO_3 sensor. Thereby, the distinct advantage of filters is the exploitation of additional and complementary molecular properties (*e.g.*, size, sorption affinity), often not accessible by sensors alone. By using advanced materials (*e.g.*, microporous metal–organic frameworks, MOF) and material design on the nanoscale (*e.g.*, heterostructures, nanocluster dopants), filters can be designed systematically to achieve high sensor selectivity. Most importantly, filters can be modular to the sensor and thus flexibly combined with different sensor technologies (*e.g.*, optical,[69] chemoresistive,[71] electrochemical[72]) and even sensor arrays.[73]

Here, we systematically review sorption, size-selective and catalytic filters with guidelines for their design in assembling highly selective sensor systems. Selectivity improvement by filters comes at increased complexity of the sensing system and each filter type introduces distinct advantages and disadvantages, broadly summarized in Table 1. We address these characteristics by first introducing the underlying filter concepts and basic principles necessary for analyte separation. Then, specific implementations of such filters are presented, highlighting trends and critically comparing their performance. Finally, device integration and performance in practical cases are elaborated. We close by highlighting current challenges and opportunities.

2. Sorption filters

Definitions & principles

A sorption filter exploits the difference between analytes flowing or diffusing through. So mixtures of analytes either adsorb[74] onto or are absorbed in the filter to enhance the sensor selectivity downstream. Most sorption filters are based on adsorption, while absorption dominates gas chromatography (GC)-sensor systems.

Table 1 Performance characteristic of different filter types (○, ↑, ↓ indicating no change, increase and decrease in comparison to the sensor without filter, respectively)

Filter type	Configuration	Selectivity	Flexibility for selectivity	Multi-analyte detection	Sensitivity	Analysis time	Power consumption	Size
Sorption	Packed bed	↑↑	↑	○	○	○	○	↑
	Separation column	↑↑	↑↑	↑↑	↓	↑↑	↑↑	↑↑
Size-selective	Overlayer	↑	↑	○	○	○	○	○
	Membrane	↑↑	↑↑	○	↓	↑	○	↑
Catalytic	Overlayer	↑	↑	○	↑	○	○	○
	Packed bed	↑↑	↑↑	○	○	○	↑	↑

These filters are inexpensive and modular to the gas sensor,[71] thus easy to implement and characterize. Most importantly, they are flexible as a wide range of sorbents is available to separate analytes based on polarity,[75] hydrophilicity,[71] boiling point,[76] molecular weight[68] or size.[77] A drawback is their saturation,[78] requiring replacement or regeneration by purging with clean air and/or by heating[79] that tends to prolong sensor response and recovery times. However, by combining purging and heating, adsorbents can be regenerated within minutes[80] as established for thermal desorption tubes in air quality monitoring.[81]

For adsorption, the chemical surface groups (nonpolar, polar and analyte-specific), accessible surface area and pore size distribution of the adsorbent (filter) are important (Fig. 2a). Adsorption of analytes takes place through weak (10–100 meV) and reversible physical forces (*i.e.*, van der Waals).[82] Sorption filters are often packed beds of adsorbent particles, porous granules or fibers. To characterize their adsorption capacity for certain analytes, a breakthrough curve is recorded.[83] Thereby, the analyte concentration at the filter outlet is measured for constant inlet analyte concentration and flow rate. The time for the outlet analyte concentration to reach a certain fraction (often 5%) of its inlet is defined as the breakthrough time.

Decreasing the flow rate through the filter (adsorbent) prolongs the breakthrough time linearly (Fig. 2b),[85] but typically lowers the sensor response as fewer analyte molecules reach the sensor.[87] Breakthrough time multiplied by the flow rate gives the breakthrough volume that is flow rate-independent and increases proportionally with adsorbent loading since more surface area is available for analyte adsorption (Fig. 2c).[85] However, larger filter loadings result in larger pressure drop[88] through the filter and prolong the sensor response time. Typically, the breakthrough volume is normalized with respect to adsorbent loading.[89] This material-specific property is useful in design of sorption filters and independent (for a wide range) of flow rate and adsorbent loading. At low analyte concentrations (<10 ppm), breakthrough volumes are independent of concentration, as typically seen in GC.[90] This is important for gas sensing in breath analysis or indoor air monitoring where analyte concentrations are in that range (*e.g.*, ~500 ppb acetone in breath[91] or ~80 ppb formaldehyde in indoor air[92]). But concentrations can reach also hundreds of ppm in certain conditions (*e.g.*, ethanol from cleaning products[93] or propane/butane from gas cookers), where breakthrough occurs earlier as the capacity of adsorbent is exhausted. This is shown exemplarily in Fig. 2c for adsorption of 85–539 ppm hexane on a porous non-polar polymer adsorbent with large surface area (Chromosorb 106, >700 m^2 g^{-1}).[85]

Adsorption by physical forces is temperature-dependent (van't Hoff law[94]) resulting in a steep decrease of breakthrough volumes with increasing temperature. This is shown in Fig. 2d for adsorption of hexane on a porous non-polar polymer adsorbent (Tenax TA), where increasing the temperature from 0 to 20 °C reduces the breakthrough volume by 95%.[80] Heating is used to accelerate regeneration of sorption filters (*e.g.*, packed zeolite bed[75] for CH_4 sensing within 2 h by heating to 250 °C) and control the separation of compounds by GC.[95] Another factor is relative humidity (RH) that is omnipresent in most applications (*e.g.*, up to 95% at 36 °C in exhaled human breath[96]). Adsorption of water leads to partial blocking of adsorption sites and reduces the breakthrough time, depending on adsorbent hydrophilicity. For instance, increasing the RH from 0 to 61% for weakly polar activated carbon fibers reduced the breakthrough time of benzene by 76% (Fig. 2e). In contrast, when using the non-polar polymer adsorbent Tenax TA, this time was not affected.[97]

Adsorbent materials & properties

Sorption filters preceding gas sensors are tabulated in Table 2, showing their composition, target analytes and figures of merit. First[64] sorption filters for gas sensing were carbon-based[77] (*i.e.*, activated carbon, graphene, carbon molecular sieve, carbon fiber, *etc.*) as these were well established already for vapor filtration (*e.g.*, gas masks[98]). Other important adsorbents include silica (silica gel[99] and mesoporous silica[100]), porous polymers (*e.g.*, Tenax TA[101]), activated alumina,[102] zeolites[103] and metal–organic frameworks (MOFs).[104] These feature high

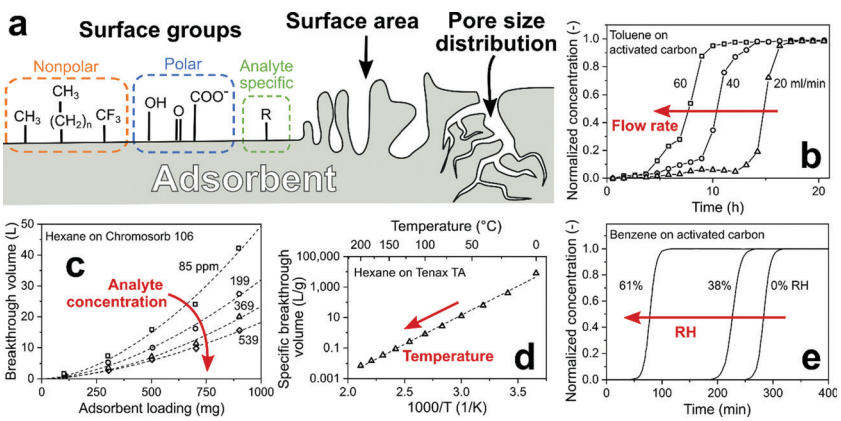

Fig. 2 (a) Critical adsorbent (filter) properties: surface chemical groups, surface area and pore size distribution. (b) Effect of overall flow rate through the filter on the breakthrough time.[84] (c) Effect of filter (adsorbent) loading and analyte concentration on breakthrough volume.[85] (d) Effect of temperature on specific breakthrough volume.[80] (e) Effect of RH on the breakthrough time.[86]

Table 2 Sorption filters in combination with gas sensors

Filter configuration	Filter material	Target analyte	Sensor	LOD[a] (ppm)	Response time	Tested interferants (selectivity)	Ref.
Packed bed	Activated carbon	CH_4	Pellistor	25 000	—	Hexamethyldisiloxane (∞^b)	59
		CO	SnO_2	20	2.5 min	Ethanol (0.11), H_2 (0.07)	76
	Ag/Al_2O_3	Ethylene	Electrochemical	0.02	10 min	Acetylene, NO, NO_2, SO_2 (all ∞^b)	141
	Carbon cloth	CO	SnO_2	15	—	Butane, ethanol, ethyl acetate, heptane (all ∞^b)	66
	Carbon cloth, charcoal granules	CH_4	Pellistor	10 000	12–50 s	Hexamethyldisiloxane (∞^b)	64
	Indigo	Ozone	Electrochemical	0.04	~5 min	NO_2 (∞^b)	143
	Indigo/carbon nanotubes	NO_2	Organic semiconductor	0.01	—	Ozone (∞^b)	145
	Zeolite 4A	H_2	SnO_2	10	—	H_2S (∞^b)	62
	Zeolite 5A	CO	Electrochemical	0.03	5 s	Ethylene (∞^b), H_2S (∞^b), CH_4 (>1000), ethane (>1000), H_2 (>1000)	65
	Zeolite MOR	CH_4	SnO_2	1000	—	Ethanol, hexane (both ∞^b)	75
Commercial GC column	Hayesep Q	H_2, CH_4	SnO_2	2	<1 min	—	158
	MXT-1	VOCs (<14 carbon atoms)	PID[c]	<0.015	30 min	—	161
	OV-1 megabore	Alcohols, acetaldehyde, acetone, ethyl acetate	In_2O_3	0.1	<5 min	—	159
	OV-101	Alkanes	TCD[d]	—	5 s	—	154
	Rtx-VMS	*cis*-1,2-Dichloroethylene, benzene, trichloro-ethylene, toluene, terachloroethylene, *p*-xylene	PID	1 μg L^{-1} (in liquid)	15 min	Various ground water compounds	157
	Rtx-5	8 organophosphates/sulfates, 5 VOCs	NEMS[e]	0.1	5 s	—	158
	Rxi-624	Benzene, ethylbenzene, toluene, xylenes	PID	0.0025	19 min	—	160
	Rtx-5MS, Rtx-200	50 VOCs	PID	—	14 min	—	162 and 163
	Rtx-VMS, Rt Q-BOND	Formaldehyde	PID	0.0005	11 min	—	155
	Not specified	Acetone	ZnO	0.1	2 min	—	156
Separation column	Activated alumina	Isoprene	Pt/SnO_2	0.005	4 s	Acetone, ethanol, methanol, NH_3 (all ∞^b)	71
	Tenax TA	Methanol	Pd/SnO_2	1	102 s	Acetone, ethanol, H_2 (both ∞^b)	68
		Ethanol, methanol	Pd/SnO_2	0.01 vol% (in liquid)	10 min	—	175
		Formaldehyde	Pd/SnO_2	0.005	2 min	Acetaldehyde, acetone, CH_4, CO, ethanol, methanol (all ∞^b)	176
Overlayer	Indigo	NO_2	Organic semiconductor	0.04	>1 h	Ozone (>20)	144

[a] Lowest measured concentration. [b] Not detectable by the sensor. [c] Photoionization detector. [d] Thermal conductivity detector. [e] Nanoelectromechanical system.

porosity and surface area (Fig. 3a–d), resulting in high adsorption capacity. They are commercially available in a variety of shapes (*e.g.*, powders, granules, pellets, fibers), specific surface areas, pore sizes and chemical functionalization (*e.g.*, surface polarity).[89] Specific surface areas range usually from 20 $m^2\ g^{-1}$ for some porous polymers (*e.g.*, Tenax GR[89]) up to 7000 $m^2\ g^{-1}$ for ultra-high surface area MOFs[105] (Fig. 3e).

Carbon-based adsorbents, silica gels, porous polymers and activated alumina typically feature a mix of meso- (2–50 nm) and micropores (<2 nm) with similar log-normal pore size distributions.[106] Zeolites[107] and MOFs,[108] on the other hand, have a well-defined micropore size in the same order of magnitude as gas molecules (*e.g.*, kinetic diameter of benzene[109] is 0.59 nm) that depends on their composition. The accessible surface area, and thus adsorption capacity, depends often on adsorbent's pore size and analyte's molecular size. For instance, *p*-xylene can access the pores of adsorbent MOF-107, while *m*- and *o*-xylene cannot, resulting in enhanced

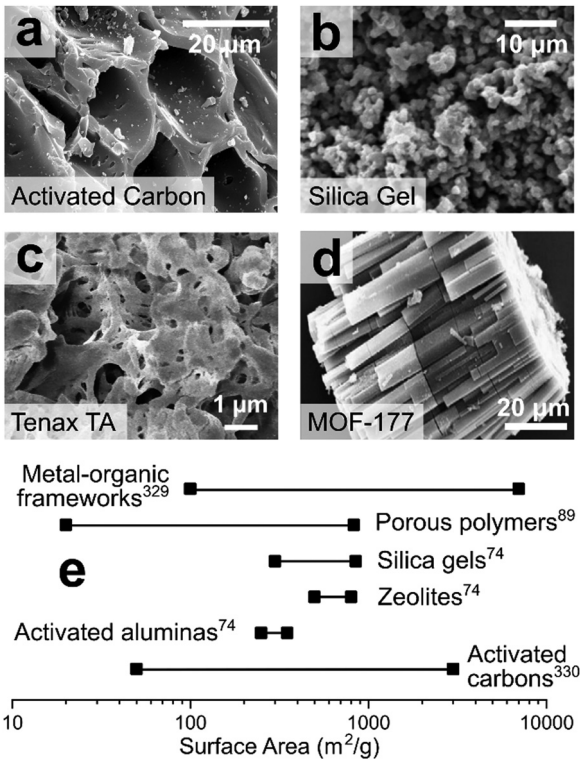

Fig. 3 SEM images of commercial adsorbents: (a) activated carbon.[118] (b) Silica gel.[119] (c) Porous polymer (Tenax TA).[68] (d) Metal–organic framework (MOF-177).[120] (a–d) Reproduced with permission. Open Access CC BY. (e) Range of surface areas for sorption materials.

adsorption capacity of *p*-xylene.[110] When applied as dense layers or membranes, such an effect can even be used to create a sharp size cut-off (*e.g.*, dehydration of solvents by zeolite membranes[111]). Also the adsorbent surface properties are crucial and can be controlled thermally (*e.g.*, higher surface area of activated carbon at higher pyrolysis temperature[112]) and chemically[113] (*e.g.*, alkali treatment of activated carbon to increase adsorption of hydrophobic VOCs,[114] plasma/microwave treatment,[115] ammonization[116] or oxidization[117]).

Sorption filters of relatively non-polar carbon-based adsorbents (*e.g.*, charcoal, activated carbon) are used to remove VOCs that interfere with the selective detection of relatively inert, non-polar gases such as H_2, CO or CH_4 (Fig. 4a). On non-polar adsorbents, VOCs are adsorbed mostly by non-specific dispersion forces that are proportional to VOC's molecular weight.[121] Such filters have been used in commercial CO sensors to meet national standards.[76] For instance, the ethanol response of a SnO_2 sensor is reduced by more than an order of magnitude with a charcoal filter (Fig. 4b, open *vs.* filled squares), in contrast to CO (circles) and H_2 (triangles) that are not affected.[76] Also other VOCs, such as butane, heptane, ethyl acetate[66] and silicones[59] are filtered out, resulting in highly selective detection of small, non-polar gases (*e.g.*, CH_4[76]).

In contrast, polar adsorbents interact with analytes mostly through dipole–dipole[122] and hydrogen bonding,[123] resulting in more specific molecule removal (*e.g.*, alcohols, carbonyls, aldehydes). Such polar adsorbents, including activated alumina,[124] silica gel,[125] P_2O_5,[126] Nafion,[127] metal–organic pastes,[128] CaCl[129] and NaOH,[130] also strongly adsorb water. So, they are used as desiccants to minimize the impact of

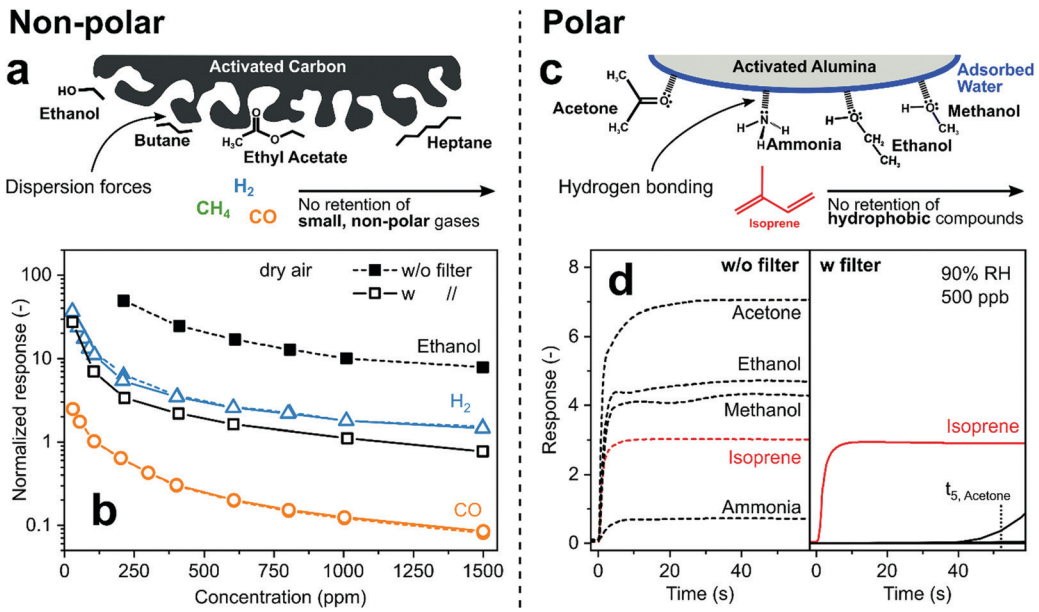

Fig. 4 (a) Concept of non-polar activated carbon VOC filter for sensing of low molecular weight gases. (b) Responses of a SnO_2 sensor to H_2 (triangles), CO (circles) and ethanol (squares) without (filled symbols) and with (open) preceding activated carbon filter.[76] Note that symbols for H_2 and CO with and without filter are on top of each other indicating that they passed unscathed through the filter that caught most (~90%) ethanol. (c) Concept of polar activated alumina filter that retains hydrophilic compounds while hydrophobic isoprene passes unhindered. (d) Response of a Pt/SnO_2 sensor to breath-relevant analytes at 500 ppb without (left panel) and with that filter (right panel).[71]

humidity that compromises sensor performance (*e.g.*, SnO_2).[131] For example, activated alumina is covered by a thin water layer in the presence of humidity[132] that adsorbs hydrophilic analytes such as alcohols, ketones and ammonia by hydrogen bonding, while hydrophobic hydrocarbons are not affected (Fig. 4c). This facilitated selective sensing of isoprene, a non-invasive marker for cholesterol and other metabolic conditions,[133] by a packed bed filter of commercial activated alumina (1 g only) upstream of a non-selective Pd/SnO_2 sensor at 90% RH.[71] While that sensor without filter is not selective (Fig. 4d), only isoprene is detected with the filter during 40 s of exposure before hydrophilic analytes break through (*e.g.*, acetone after 52 s). This is much shorter than typically obtained with carbon-based filters (>1 h[134]) due to their much higher surface area (>1000 *vs.* 155 $m^2\ g^{-1}$, for activated carbon and alumina, respectively), but sufficient for end-tidal breath measurements[135] and buffered samplers.[136] The resulting isoprene selectivity by using this filter outperforms[71] other TiO_2,[137] Ti/ZnO[138] and h-WO_3[139] sensors for isoprene.

More specific interaction includes silver ions that adsorb ethylene quite selectively due to π–π interactions.[140] This was used for selective detection of ethylene for monitoring fruit ripeness using a Ag-doped alumina filter.[141] After sampling and trapping of ethylene, it is released by heating the filter to 60 °C, and detected by a non-specific amperometric sensor without interference by NO, NO_2, SO_2 and acetylene.[141] Another example is indigo, whose reactive C=C bond selectively reacts with ozone.[142] This is used by NO_2 sensors in the form of indigo-impregnated filter paper,[143] indigo layers directly deposited on a semiconducting sensor[144] or indigo dispersed in a packed bed of carbon nanotubes[145] to mitigate interference by ozone. Using differential sensing techniques, such indigo filters were even used for selective ozone detection.[143] Such analyte-specific interactions were obtained also during formation of chemical complexes,[146] for instance, ammonia with CaCl[147] or CuBr[34] forming $Cu(NH_3)_2^+$. The first was used to reduce ammonia concentrations in breath from 10 ppm to only 0.8 ppm while other breath analytes were not influenced.[129] The second has been applied for sensing ammonia down to 5 ppb at room temperature and 90% RH,[148] but could be used as filter as well. Also quite promising for sorption filters is chemical derivatization, used for instance for selective removal of aldehydes in gas mixtures (*e.g.*, indoor air) by 2,4-dinitrophenylhydrazine.[4] Another option is surface acidity/basicity tuning for preferential adsorption of bases/acids (*e.g.*, acetic acid on basic Y/ZnO[149]).

Analyte separation in time

Sorption filters can also act as GC columns to separate analytes in time rather than remove them completely.[150] For this, the analyte-containing gas sample is carried through the filter by a gas (*e.g.*, helium, nitrogen and rarely air) with a pump or pressurized gas cylinder. Most GC-sensor systems (partition or gas–liquid GC)[95] use open tubular columns (coated with a liquid phase on the inside),[150] which are heated to control analyte separation.[151] If the elution (retention) times of analytes are quite apart, analytes can be detected sequentially by the sensor resulting in very high selectivity and multi-analyte detection capacity (*e.g.*, H_2 and CH_4 in breath[152]). An inherent drawback of GC-sensors is their batch nature, preventing continuous monitoring of analytes. However, by miniaturizing GC-systems for low sample and dead volumes and optimizing column heating protocols, analysis time can be reduced to a few seconds.[153]

The first GC-sensor systems were combinations of GC columns with a portable gas sensor.[154] They selectively detected a variety of analytes, including formaldehyde,[155] breath acetone,[156] VOCs from groundwater headspace,[157] H_2 and CH_4,[158] alcohols[159] and aromatics[160] with limits of detection as low as 15 ppt.[161] Even highly complex mixtures of up to 50 analytes[162] could be separated by 2-dimensional GC techniques (two columns in series) with validated performance for occupational exposure monitoring.[163] Such GC-sensor systems are available commercially, for instance the Defiant TOCAM[164] or Dräger X-pid[165] for broad chemical analysis or the Quintron Breath Tracker[152] for breath H_2 and CH_4 in the diagnosis of lactose malabsorption. However, such systems are expensive (several hundred dollars for the column alone), bulky (coiled column of several meters length), heavy (several kg) and require high power (for heating of the column), making them not suitable for battery-powered and handheld detectors.

Micro GC-sensor systems can be based entirely on microelectromechanical systems (MEMS)[166] using planar (*i.e.*, microchip) GC columns,[154] resulting in much smaller and portable systems, *i.e.*, mountable on a belt[167] (Fig. 5a). Such systems can reach separation performance close to benchtop GCs, as illustrated in Fig. 5b where 21 different VOCs are separated within 200 s by a GC-flame ionization detector (FID, red chromatogram) and the micro GC-sensor system (blue chromatogram).[167] They have been tested with a variety of analyte mixtures, including indoor air pollutants,[168] lung cancer biomarkers,[169] chemical warfare agents,[170] aromatics,[171] trichloroethylene in indoor air,[172] explosive markers[173] or VOCs for workplace exposure safety.[174] However, GC-sensor devices with proven performance under real conditions validated with a benchtop device (*e.g.*, as shown in Fig. 5c for personal exposure monitoring of trichloroethylene with a GC-FID and the belt-mounted GC-sensor device[167]) are rare.

Simpler implementation is achieved by focusing on single analytes for specific applications. An example is a detector consisting of a non-specific Pd/SnO_2 gas sensor and a compact separation column for screening of methanol in alcoholic beverages and exhaled breath to detect liquor adulteration and diagnose methanol poisoning non-invasively.[68] The detector is handheld (94 g), fully integrated, inexpensive and can communicate results by Wi-Fi to a smartphone (Fig. 5d).[175] It uses a compact packed bed (4.5 cm long, 4 mm diameter) of commercial Tenax TA sorbent with room air as carrier gas instead of a capillary or microchip GC column.[68] As a result, methanol is detected selectively in the headspace of alcoholic drinks laced with 1 vol% methanol within 2 min (Fig. 5e).[175] After flushing the column with room air for 10 min,[68] it is fully regenerated and ready for the next measurement. The device revealed harmless from harmful concentrations of methanol

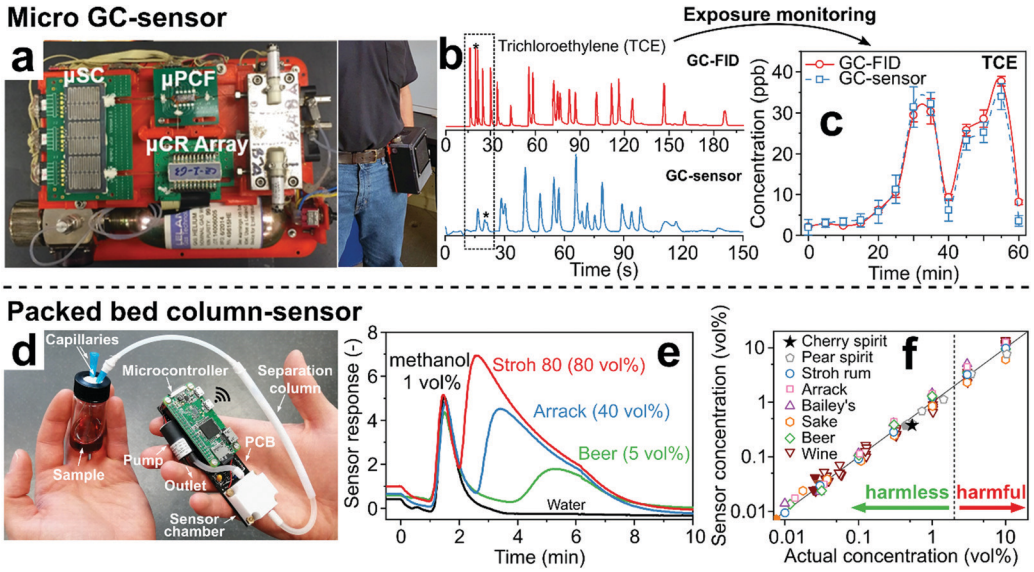

Fig. 5 (a) State-of-the-art micro GC-sensor system consisting of micropreconcentrator-focuser (μPCF), microseparation column (μSC) and micro-chemiresistor array (μCR array) that can be mounted on a belt. Reproduced with permission.[167] Copyright 2019 American Chemical Society. (b) Chromatograms of a mixture of 21 VOCs by a benchtop GC-FID and by the micro GC-sensor system showing similar separation performance for both systems.[167] (c) Selective monitoring of trichloroethylene over 60 min by a belt-mounted micro GC-sensor system (dashed line) in comparison to measurements by benchtop GC-FID (solid line).[167] (d) Handheld analyzer for measurement of methanol in laced beverages. Reproduced with permission.[175] Copyright 2020 Springer Nature. (e) Sensor response after sampling of Stroh 80, Arrack, beer and water laced with 1 vol% methanol.[175] (f) Scatter plot of the sensor-measured methanol concentrations *versus* the actual concentration for beverages laced with harmless and harmful methanol concentrations.[175]

down to 0.01 vol% in different wines, beers and liquors from six continents (Fig. 5f).[175]

This concept of simple packed bed separation columns can be adapted easily to other applications. For example, using a larger (500 mg) Tenax TA separation column, formaldehyde was measured within 2 min at concentrations as low as 5 ppb at 40% RH without interference by H_2, CH_4, CO, methanol, acetaldehyde, ethanol, and acetone. As a result, ppb-level formaldehyde concentrations were detected for the first time in wood-product emissions and in indoor air with a low-cost solid-state sensor.[176] This is possible by the very high selectivity provided by the simple and modular packed bed sorption column, which cannot be reached typically by sensors alone (*e.g.*, ZnO/ZIF-8 core–shell structures,[177] NiO–SnO_2 microflowers[178]) or their arrays (*e.g.*, four SnO_2-based sensors[138]).

3. Size-selective filters

Definitions & principles

Size-selective filters separate analytes by their kinetic diameter. These filters are microporous[179] with pore sizes (usually <2 nm) comparable to analyte diameters. If applied as membranes in front of the sensor, analytes larger than the pore size are blocked (*i.e.*, size cut-off) from reaching the sensor (Fig. 6a). This can result in very high selectivity to target analytes over hundreds of interferants typically present in such mixtures (*e.g.*, VOCs in indoor air[180] such as terpenes, alkenes, aromatic hydrocarbons). A drawback of such filters is their ineffectiveness for interferants smaller than the target analyte, which can be addressed by combination with other filter types or selective sensing materials. All size-selective filter–sensor systems are tabulated in Table 3 together with various figures of merit for comparison.

Most promising microporous materials are zeolites,[185] MOFs[186] and covalent organic frameworks[187] (COF) featuring pore sizes that depend on crystal structure and composition. An advantage is the myriad of available frameworks (*e.g.*, 248 zeolites,[107] thousands of MOFs and COFs[188]) offering distinct pore sizes that can be matched flexibly to target analytes. This is illustrated in Fig. 6b, showing the kinetic diameters of common analytes in gas sensing and the pore size of selected zeolites (red) and MOFs (blue). Because of their high internal surface area and intrinsic microporosity, zeolites and MOFs are used frequently for catalysis[189] (*e.g.*, production of styrene with zeolite ZSM-5 catalyst[190]), gas storage[191] (*e.g.*, H_2 in MOF Cu-EMOF[192]) and even sensors (*e.g.*, chemoresistive[54] or optical[193] MOFs and zeolites[58]).

The selectivity of such filters is characterized by the analyte permeance (molar flux per unit driving force).[194] The permeance strongly depends on analyte size as shown in Fig. 6c exemplarily for a zeolite (SSZ-13) membrane with 0.38 nm pore size (dashed line).[182] In fact, H_2 (0.28 nm) features almost three orders of magnitude higher permeance than SF_6 (0.55 nm). However, differences in adsorption strength between analytes can influence the permeance.[195] For instance, CO_2 preferentially adsorbs on SSZ-13, hindering diffusion of other compounds in gas mixtures through the zeolite.[182]

A key property of size-selective filters is their thickness that is inversely proportional to analyte permeance, as shown

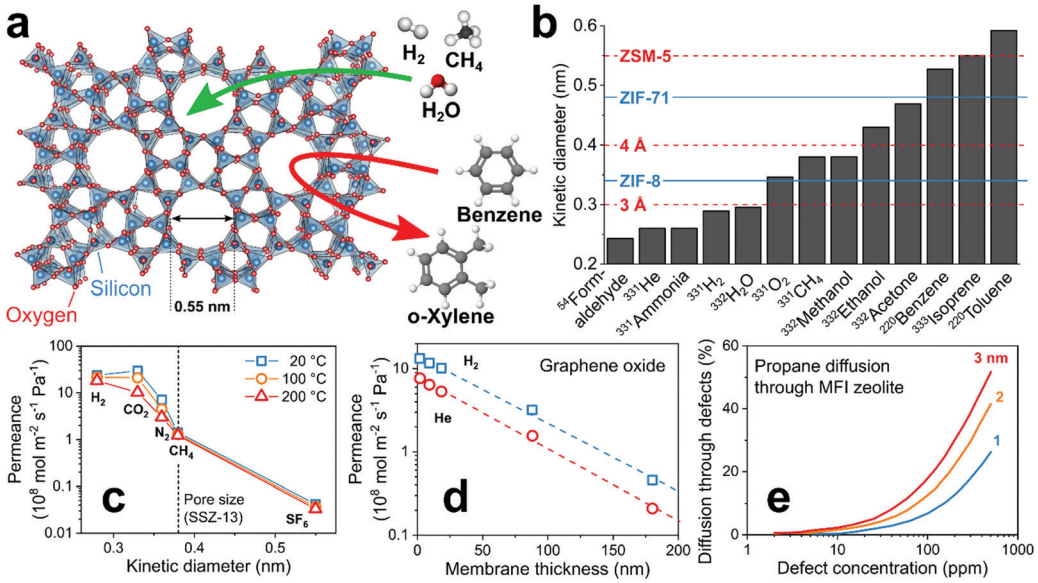

Fig. 6 (a) Working principle of a size-selective zeolite filter. Arrows indicate blocked (red) and possible (green) diffusion through the microporous structure. (b) Kinetic diameters of common analytes in gas sensing and pore sizes of commonly used zeolites[107] (dashed lines) and MOFs[181] (solid lines). (c) Effect of analyte kinetic diameter on membrane permeance at three temperatures.[182] (d) Effect of membrane thickness on permeance.[183] (e) Effect of membrane defect size and concentration on diffusion of analytes through such defects.[184]

exemplarily for H_2 and He on 1.9–180 nm thick microporous graphene oxide (GO) layers (Fig. 6d).[183] Thus, thin layers are needed for fast sensor responses. This often comes at the cost of higher defect density (*e.g.*, cracks or pinholes), compromising separation selectivity since analytes can pass through the defects. The relation between defect concentration and diffusion is shown in Fig. 6e for propane and zeolite MFI membranes.[184] Even extremely low defect concentrations reduce drastically analyte selectivity.[184] Thus, a major challenge for effective size-selective filters is the synthesis of thin and defect-free ones (*e.g.*, MOFs,[196] zeolites[184] and GO[197]). Mixed matrix membranes (MMM)[198] that consist of a microporous material dispersed in a polymer matrix are promising also. The MMMs can be easily processed to thin membranes with a small number of defects, resulting in high permeance while preserving selectivity.

Pore-size control

First size-selective filters were layers of amorphous SiO_2 directly on top of sensing films (*e.g.*, SnO_2,[199] Ga_2O_3,[200] WO_3[201] or In_2O_3[202]). These were obtained at elevated temperature (>500 °C) under exposure of the sensing film to a silicone source (*e.g.*, hexamethyldisiloxane).[203] The resulting microporous SiO_2 layer is impenetrable for most analytes except for very small H_2, resulting in a more than 100 times higher H_2 selectivity[204] to VOCs (*e.g.*, ethanol, acetone and benzene). This is remarkable for chemoresistive H_2 sensors, which offer low limit of detection (*e.g.*, 10 ppb by CeO_2/In_2O_3[205]) that is critical for leak detection,[206] but typically suffer from poor selectivity[207] (*e.g.*, <13 to CO for that sensor[205]). However, the introduced diffusion barrier also increased response and especially recovery times of sensors from seconds to several minutes[208] or even hours[209] depending on SiO_2 thickness. This is too long for most applications (*e.g.*, seconds for leak detection[210]).

Capitalizing on the effect of filter layer thickness on analyte permeance (Fig. 6d), SiO_2 layers with graded thickness[211] had also been deposited on chemoresistive microarrays, allowing slight selectivity modulation from sensor to sensor. While individual sensors remain unspecific, different analytes (*e.g.*, formaldehyde, CO, ammonia, acetone, *etc.*) were distinguished by pattern analysis in offline breath analysis[212] and air quality monitoring.[213] The pore size and shape of SiO_2 can even be adjusted flexibly by molecular imprinting of adsorbed molecules as template during deposition.[214] For instance, templating such layers on SnO_2 sensors with benzaldehyde resulted in high selectivity to linear hexane over its branched isomers.[215] Templating with smaller butanal, however, reduced responses to all analytes.[215]

Other microporous materials allow even more flexible control over pore size to adjust selectivity. For instance, pristine graphene oxide (GO) membranes have a narrow pore size distribution <0.3 nm[216] that is typically adjusted (*i.e.*, size and density) by physical (*e.g.*, ion-bombardment[217]) and chemical treatments (*e.g.*, oxidative etching[218]). Such dense and porous GO membranes with small (0.3–0.4 nm) and large (0.5–0.6 nm) pores were placed upstream of PdO/WO_3 sensors for selective detection of H_2S (Fig. 7a).[219] The sensor with dense GO layer (Fig. 7b, squares) showed lower H_2S selectivity and sensitivity than the sensor alone (circles), as all analytes cannot pass the small intrinsic GO pores. For GO layers with large (triangles) and small (diamonds) pores, the H_2S selectivity is increased to formaldehyde and large analytes (*i.e.*, ethanol, acetone and toluene 0.59 nm[220]) compared to the sensor alone. For instance, the selectivity to acetone is tripled (from 4.7 to 14)

Table 3 Size-selective filters in combination with gas sensors

Filter configuration	Filter material	Target analyte	Sensor	LOD[a] (ppm)	Response time	Tested interferants (selectivity)	Ref.
Overlayer	PMMA	H_2	Plasmonic	10	<1 s	CH_4 (63), CO_2 (32), CO (2.1), NO_2 (0.12)	69
	SiO_2	H_2	SnO_2	20 000	—	CH_4 (>1000)	199
				50	60 s	Butane (>500), CH_4 (>500), CO (>500), ethanol (18), methanol (11)	203
				1000	<1 min	Acetone, benzene, ethanol (all >1000)	204
				3100	>1 min	CH_4, propane (both >1000)	208
				0.250	>1 h	CH_4 (>100), ethanol (>100), CO (>50)	209
			Ga_2O_3	500	<30 s	Acetone, CH_4, CO, CO_2, ethanol, isobutene, propane, NH_3, NO	200
			In_2O_3	100	5 s	CH_4 (>100), isobutane (12), CO (6.8), ethanol (<1)	202
	MOF ZIF-8	Formaldehyde	ZnO	10	21 s	Toluene (>100), acetone (10.6), ethanol (7.4), methanol (6.5), NH_3 (5.1)	177
		H_2	ZnO	10	—	Benzene (12), NH_3 (4.2), acetone (3.1), ethanol (2)	181
				10	>5 min	Benzene, toluene (both ∞[b])	220
				5	>5 min	CO (37)	227
			Pd/ZnO	10	>5 min	Acetone, benzene, ethanol, toluene (all ∞[b])	228
	MOF ZIF-71	H_2S	WO_3	2	2 min	Ethanol (19), acetone (11), NO_2 (3.4)	230
		H_2	ZnO	20	—	Acetone (1.9)	234
		Ethanol	ZnO	10	—	Benzene (27), NH_3 (13), H_2 (3.7), acetone (1.3)	181
	Zeolite FER	CO	La_2O_3–Au/SnO_2	50	—	Isopropanol (20), ethylene (15), ethanol (13), H_2 (9)	237
	Zeolite LTA	NO	$Zn_{1-x}Cu_xO$	0.050	<1 min	Acetone, CO_2, ethanol, H_2, NH_3	239
		Ethanol	Pd/SnO_2	10	1.7 min	CH_4 (>1000), propane (>400), CO (>100), H_2 (>100)	236
				20	16 min	H_2O (>4000), CH_4 (>200), propane (74), CO (35), H_2 (31)	223
			WO_3, Cr_2TiO_5	21	>30 min	CO (>1000)	238
	Zeolite MFI	Ethanol	Pd/SnO_2	20	3 min	H_2O (>1000), CH_4 (>100), propane (83), CO (6.2), H_2 (2.2)	223
			WO_3, Cr_2TiO_5	21	>5 min	CO (>100)	238
	Zeolite FAU, BEA, MOR	Acetone, ethanol, NH_3, NO_2	ZnO	1	—	—	240
	Mix. (LTA, FAU, MFI)	—	SnO_2	2.5	<5 min	Acetone, butane, CO, ethane, ethanol, isopropanol, propane, toluene	241
Overlayer (graded thickness)	SiO_2	CO	WO_3	100	—	—	201
		Acetone, CO, isopropanol	Pt/SnO_2	0.5	—	—	211
		H_2S, NH_3	WO_3	0.2	>1 min	Ethanol, H_2O	212
		Indoor air contaminants	SnO_2, WO_3	<1	<5 s	—	213
Overlayer (patterned)	SiO_2	Alcohols, aldehydes	SnO_2	—	—	—	214
		Hexane	SnO_2	—	>1 min	2,2-Dimethylbutane (>82), 2-methylpentane (82)	215
Membrane	Graphene oxide	H_2S	PdO/WO_3	1	30 s	Acetone (14), NH_3 (14), formaldehyde (13), ethanol (11), toluene (11), methanethiol (4)	219
	Zeolite MFI	Formaldehyde	Pd/SnO_2	0.03	8 min	Ethanol (>1000), isoprene (>1000), methanol (>1000), NH_3 (>1000), TIPB (>1000), acetone (>100)	242

[a] Lowest measured concentration. [b] Not detectable by the sensor.

by covering the sensor with a GO layer having small pores, while response and recovery times did not change much. However, analytes smaller than the pore size (*i.e.*, ammonia 0.29, H_2S 0.36 and methanethiol 0.45 nm) can pass through the pores more easily, so the H_2S selectivity is increased less. The exception is formaldehyde (0.23 nm), probably due to its preferential adsorption[221] on GO. Overall, the obtained H_2S selectivity is only moderate (<15 over ammonia and ethanol) and surpassed by other chemoresistive H_2S sensors (*e.g.*, >700 over ammonia and ethanol by CuO[222]). However, these modular GO layers could be combined readily also with other, more selective H_2S sensors.

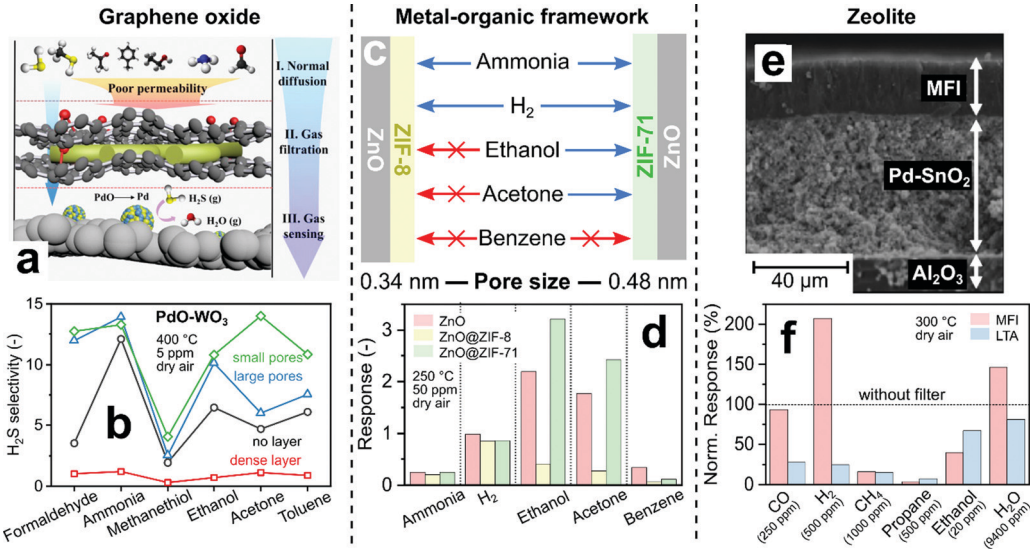

Fig. 7 (a) Concept for H_2S selective sensor by GO filter membrane. Reproduced with permission.[219] Copyright 2020 American Chemical Society. (b) H_2S selectivity over various confounders of a PdO-doped WO_3 sensor with GO filter membranes.[219] (c) Pore size-dependent selectivity of ZnO nanorods covered by metal–organic frameworks ZIF-8 and ZIF-71. Arrows indicate if an analyte's diameter is smaller (blue) or larger (red) than the MOF pores. (d) ZnO sensor response without (red) and with ZIF-8 (yellow) or ZIF-71 (green) MOF overlayers.[181] (e) Cross-section image of a Pd-doped SnO_2 sensing film on Al_2O_3 support coated with MFI zeolite. Reproduced with permission.[223] Copyright 2007 Elsevier. (f) Pd/SnO_2 sensor responses with hydrophobic MFI or hydrophilic LTA overlayers normalized to sensor responses without filter (line).[223]

Zeolites and MOFs feature very narrow pore size distributions. While MOFs have been used as selective sensor materials (*e.g.*, interference[224]- or luminescent[225]-based), the first implementation as auxiliary size-selective filters were ZIF-8 layers directly grown on ZnO nanowire sensors operated at 300 °C.[220] The ZIF-8 membrane features pore openings of 0.34 nm,[226] smaller than most analyte diameters (Fig. 6b). While the sensor without filter showed low (<5) H_2 selectivity to toluene and benzene, their responses are completely blocked by the ZIF-8 layer irrespective of their concentration, resulting in high H_2 selectivity. Using ZIF-8 as filter also blocked CO,[227] ethanol[228] and acetone.[228] These results outperform even SiO_2-covered sensors, especially as response and recovery times are unscathed due to the very thin (2–3 nm[228]) ZIF-8 thicknesses. They are only outperformed by other sensor technologies such as optical nanoplasmonic sensors,[229] which however typically suffer from higher detection limits ($\sim$100 ppm[229]).

By using MOFs with different pore sizes, the selectivity can be changed drastically using the same sensor, as shown exemplary in Fig. 7c and d for MOF-coated ZnO nanorods.[181] With ZIF-8 coating (Fig. 7d, yellow bars), most of ammonia and H_2 pass through, giving similar responses to bare sensors (red bars, reduced by $<$20%). The responses for larger analytes (*i.e.*, ethanol, acetone and benzene), however, decreased by a factor of 4–6. In contrast, for ZIF-71 coatings with larger pore opening (0.48 nm, green bars), ethanol and acetone pass through and even show slightly higher sensor response than the uncoated sensor. Such increased responses were also observed for H_2S on ZIF-71 covered WO_3 sensors[230] and were attributed to enhanced analyte adsorption onto the ZIF-71.[231]

Besides framework composition, the pore size of MOFs[232] and zeolites[233] can also be adjusted by encapsulation of ions or nanoparticles in their pores. For instance, the selectivity of a ZnO sensor coated with ZIF-71 was tuned by incorporation of silver nanoparticles.[234] With increasing nanoparticle size and concentration, the response to acetone decreased by 64%, while that to H_2 increased by 83%.[234] These results show how size-selective filters enable the control of sensor selectivity based on analyte size – otherwise impossible by sensor materials, arrays or other filter types that interact mostly chemically with the analytes.

Fig. 7e and f shows the effect of different zeolite frameworks on the selectivity of a Pd-doped SnO_2 sensor operated at 300 °C in dry air.[223] MFI and LTA zeolite layers ($\sim$25 µm thickness with pore sizes 0.47 and 0.42 nm,[107] respectively) were grown directly on screen-printed sensors (Fig. 7e) by seeding their surface with zeolite crystals and subsequent solvothermal synthesis.[235] Fig. 7f shows the response with MFI (red bars) and LTA (blue bars) to different analytes normalized to the response without zeolite layer. While this sensor is non-specific, by adding an MFI layer, it responds selectively to H_2, CO and H_2O. In contrast, LTA increased primarily the selectivity to ethanol and H_2O. Both layers significantly reduced the responses to propane and CH_4, but also increased response times from 38 s to 3 and 16 min with LTA and MFI layers, respectively. The selectivity changes were mostly attributed to zeolite adsorption characteristics (LTA is hydrophilic and MFI hydrophobic) and not to size-selective diffusion, as the zeolite layers showed a large number of intra-crystalline voids (*i.e.*, defects leading to unselective diffusion as shown in Fig. 6e). Layers with similar performance were prepared also by simple micro-dropping of zeolite suspensions directly on sensors to preserve their film integrity.[236]

A variety of zeolites coated on different sensors (*e.g.*, FER on Au–La_2O_3/SnO_2,[237] LTA and MFI on WO_3,[238] Cr_2TiO_5[238] and $Zn_{1-x}Cu_xO$,[239] array of FAU, BEA and MOR on ZnO[240] and mixtures of LTA, FAU and MFI on SnO_2[241]) showed a modulation of sensor response. For instance, ethanol selectivity over isopropanol of SnO_2 sensors was improved from 1.0 to 4.2 by covering with ~26 μm of MFI zeolite.[241] However, the achieved selectivities were only moderate (<20), in the range typically observed for different sensor compositions without the need for filters and not yet suitable for low concentration analyte detection in complex mixtures (*e.g.*, breath or indoor air). Furthermore, the selectivity improvements often cannot be attributed to size-selective filtering alone. In fact, they are often a complex interplay between (i) diffusion resistance, (ii) size-selectivity, (iii) preferential adsorption as a result of different filter surface properties (Section 2) and (iv) catalytic effects as a result of the thermal coupling of filter to the (typically) heated sensor (Section 4).

Filter configuration

Size-selective filters can be implemented as direct coatings (*i.e.*, overlayer)[237] or as membranes (free-standing[219] or on a macroporous support[242]) placed in front of sensors. Both configurations offer distinct dis/advantages as shown here exemplarily with two filter–sensor systems for selective formaldehyde detection:

The first system uses a ZIF-8 MOF overlayer (~200 nm thick) directly formed on a ZnO sensor (Fig. 8a).[177] While such coating of sensors with size-selective materials is attractive to maintain a compact sensor configuration, it leads to elevated filter temperature through its contact with the heated sensor (here 300 °C). This often degrades the size-selectivity as most microporous materials are catalytically active.[243] The ZnO sensor without filter is mostly non-selective, giving high responses to a variety of analytes (Fig. 8b). With filter layer (Fig. 8c), responses to formaldehyde and ammonia, that are smaller than the ZIF-8 pores, are reduced only slightly. Also the sensor response times stay similar (14 to 21 s) because of the thin (~200 nm) filter layer. Large molecules such as toluene are blocked by the filter, resulting in pronounced formaldehyde selectivity >100, even in the presence of high humidity (>90% RH). However, other analytes larger than the pore size (*i.e.*, methanol, ethanol and acetone) are not held back, probably because of catalytic conversion[244] to smaller molecules on the heated ZIF-8 layer interacting with the ZnO. As a result, only moderate selectivities (5–11) are achieved that might be insufficient for measurement of formaldehyde in indoor air where interferant concentrations can be orders of magnitude higher.[245] However, such size-selective ZIF-8 layers could be combined with other formaldehyde-selective sensors (*e.g.*, $In_4Sn_3O_{12}$,[30] NiO–SnO_2,[178] Co/In_2O_3[246] or ZnO quantum dots loaded hollow SnO_2 nanospheres[247]) or sensor arrays[138] to further boost their selectivity. Alternatively, size-selective overlayers can be applied on room temperature sensors to avoid catalytic conversion of interferants.

In contrast, size-selective membrane filters can be produced individually with good control over morphology (*e.g.*, thickness[248]) and can be combined as separate units more flexibly with sensors (*e.g.*, electrochemical, optical). Fig. 8d–f shows an example where a size-selective membrane of MFI zeolite was formed on a macroporous Al_2O_3 support (Fig. 8d) and placed upstream of a Pd-doped SnO_2 sensor.[242] Similar to uncoated ZnO, the Pd-doped SnO_2 sensor (Fig. 8e) alone is not selective. In contrast to the overlayer, however, the membrane features a size-cutoff, as analytes larger than the pore size (*i.e.*, isoprene and TIPB) are barely detected by the sensor (Fig. 8f). Interestingly, also smaller analytes (*i.e.*, methanol, ethanol, acetone and ammonia) are blocked effectively by the membrane, probably as a result of adsorption effects. So, excellent formaldehyde selectivity up to more than 1000 is

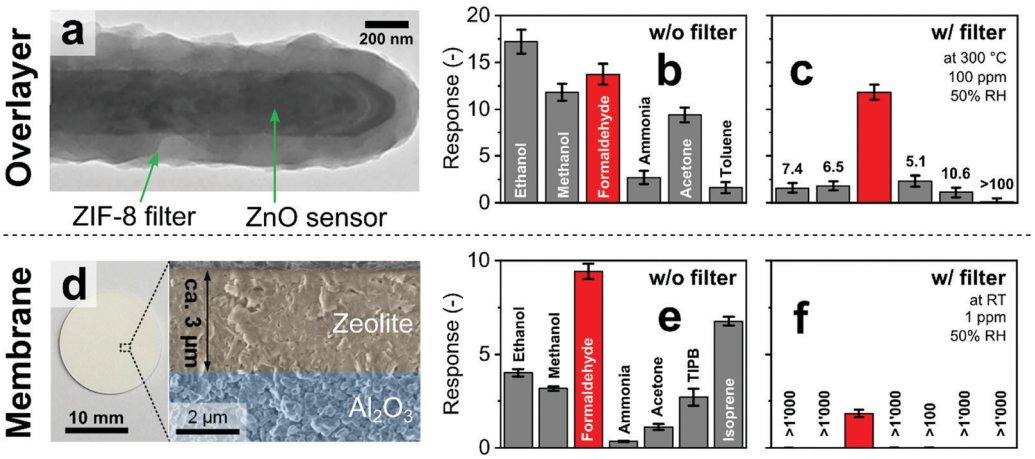

Fig. 8 (a) ZnO sensing nanorods covered by a microporous overlayer of ZIF-8 MOF. Reproduced with permission.[177] Copyright 2016 American Chemical Society. Sensor response without (b) and with ZIF-8 overlayer (c) to indoor air-relevant analytes with the corresponding formaldehyde selectivities.[177] (d) Microporous MFI zeolite membrane grown on a macroporous alumina substrate. Reproduced with permission.[242] Copyright 2018 Elsevier. Response of a Pd-doped SnO_2 sensor without (e) and in combination with MFI zeolite membrane (f) to indoor air-relevant analytes with corresponding formaldehyde selectivities.[242]

achieved even at low concentrations down to 30 ppb at 90% RH, unmatched by most chemoresistive sensors. A drawback of this configuration, however, is the larger zeolite thickness (~3 μm) that introduces a high diffusion resistance. As a result, the formaldehyde response is reduced by a factor of 5 and the response and recovery times increased to 8 and 72 min,[242] respectively, significantly higher than those with overlayers (Fig. 8a–c).[177]

4. Catalytic filters

Definitions & principles

Catalytic filters exploit differences in chemical reactivity between analytes to enhance the selectivity of downstream sensors. Ideally, the target analyte passes the filter intact, while interferants convert fully on the filter (catalyst) to inert species undetected by the sensor, as illustrated in Fig. 9a. Nevertheless, partial analyte conversion and formation of intermediates has been observed.[249] As a result, interferants are eliminated or their concentration is reduced substantially, resulting in high sensor selectivity. Most importantly with respect to other filters, catalytic ones operate continuously[250] (and do not saturate like sorption filters, Section 2). This is a distinct feature if interferants are present constantly in the background air (*e.g.*, ethanol from cleaning products[93] or disinfectants[251]). However, catalytic filters usually require some heating to optimize selectivity, which can be circumvented if the catalytic filter is deposited directly onto the heated sensing film as an overlayer.

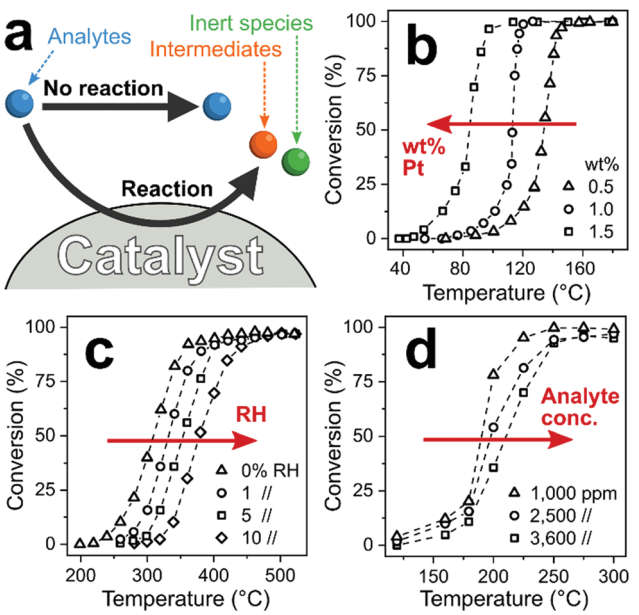

Fig. 9 (a) Chemical reaction pathways between analytes and catalytic filter. Analytes thereby pass the catalyst unscathed without reaction (desired for the target analyte) or are converted to intermediate or inert species (desired for interferants). (b) Increased noble metal loading lowers filter temperature for complete conversion.[252] (c) Increased RH[253] and (d) analyte concentration[254] increases that temperature.

A variety of crystalline[255] or amorphous[256] catalytic materials is available from heterogeneous catalysis, including metal oxides,[257] mixed-metal catalysts,[258] zeolites,[189] mesoporous silica[189] and MOFs.[259] They typically feature high specific surface areas (*e.g.*, >100 m^2 g^{-1})[260] with surface composition, structure and operational temperature determining the overall reactivity, and subsequently, selectivity. These properties make catalytic filters attractive for material engineering at the nanoscale (*e.g.*, surface area,[261] acidity[262] or surface hydrophobicity[263]). In particular, noble metals (*e.g.*, Pt,[264] Pd,[264] Rh,[264] Au[258] and Ag[261]) are frequently added to enhance reactivity by tuning their size down to single atoms.[265] For example, increasing the loading of Pt on Al_2O_3 from 0.5 (triangles, Fig. 9b) to 1.5 wt% (squares) reduces the temperature of full propene combustion from 160 to 100 °C.[252]

In contrast to heterogeneous catalysis, catalytic filters for sensors are typically operated in mixtures with many compounds (*e.g.*, several hundred in human breath[266]), low analyte concentrations and high or varying humidity. These parameters markedly influence the reactivity and selectivity of catalytic filters. For example, catalyst activity is strongly influenced by humidity as water molecules can competitively interact and block catalyst active sites,[267] reducing their reactivity. As an example, the onset of CH_4 conversion on Pd/SnO_2 shifts from 240 °C in dry air to 320 °C at just 10% RH (Fig. 9c).[253] For sensor applications, humidity often varies greatly (*e.g.*, 30–95% RH[268] in indoor air) or is present at high levels (*e.g.*, exhaled breath >97% RH[96]), which needs to be considered in the design of catalytic filters. Furthermore, analyte concentration influences conversion at high concentrations when the reaction kinetics (*i.e.*, diffusion to, adsorption on, conversion at and desorption from the catalyst) become rate-limited.[269] For instance, on Pt/Al_2O_3–CeO_2, complete conversion of 1000 ppm toluene is attained at 250 °C, while for 3600 ppm it is 300 °C (Fig. 9d).[254] For gas sensors, the catalytic filter needs to convert interferants at high concentrations and leave intact the target analyte often present at orders of magnitude lower concentration (*e.g.*, <10 ppb formaldehyde in indoor air[92] with >10 ppm H_2, ethanol or acetone[245]). So, heterogeneous catalysis can inspire the design of catalytic filters, but their performance needs to be tailored systematically to sensor conditions.

Tailored selectivity

Sensors with catalytic filters are tabulated in Table 4, showing their composition, target analytes and various figures of merit. First catalytic filters for gas sensors were developed to remove VOCs (*e.g.*, CO and ethanol) for reliable alkane detection.[250] Monitoring alkanes (*e.g.*, CH_4, propane and butane) in domestic[270] and industrial areas (*e.g.*, from gas leaks[271] and coal mines[272]) is important due to their high flammability[273] and regulated exposure limit (*e.g.*, CH_4, 1000 ppm[274]). This is challenging, as chemoresistive sensors respond weakly to alkanes (high energy needed to activate C–H bonds[254]) and suffer from high cross-sensitivity[275] to pollutants, particularly CO (*e.g.*, >7000 ppm in coal mines[276] and >100 ppm in industrial areas[277]) and ethanol (*e.g.*, >100 ppm from hand disinfection[251]).

Table 4 Catalytic filters in combination with gas sensors

Filter configuration	Filter material	Target analyte	Sensor	LOD[a] (ppm)	Response time	Tested interferants (selectivity)	Ref.
Overlayer	Al_2O_3	CH_4	Pellistor	25 000	—	Hexamethyldisiloxane (<1)	59
	Co_3O_4	Benzene	Pd/SnO_2	0.25	3 s	Ethanol (5.1), xylene (4.8), toluene (2.6), CO (2.4), formaldehyde (2.4)	300
	CuO	CO	SnO_2	900	—	Ethanol (<1)	308
	Cr_2O_3	Ethylene	SnO_2	0.1	9 s	NH_3 (24), dimethylamine (17), formaldehyde (6.3), ethanol (5.7), CO (4.3), trimethylamine (3.4)	312
	Ga_2O_3	CH_4	Ga_2O_3	500	—	Ethanol (2), acetone (<1)	286
	Zeolite MFI	CO	Pd/WO_3	100	—	Acetone, ethanol, methanol (all <1)	305
	SnO_2, TiO_2	Toluene, xylene	Co_3O_4	5	<6 min	Formaldehyde (>20), CO (>10), benzene (>8), ethanol (>7.6)	303
	Pt	CO	SnO_2	10	—	NO_2 (<1), ozone (<1)	310
		Propane	$In_{0.1}Sb_{0.005}Pd_{0.1}/SnO_2$	500	—	CO (40), ethanol (<1)	73
	Pd	Propane	$In_{0.1}Sb_{0.005}Pd_{0.1}/SnO_2$	500	—	CO (>1000), ethanol (1)	73
	Pd, Ag	CO, H_2	SnO_2	1000	—	Ozone (<1)	307
	Pt/Al_2O_3	CH_4, ethane	SnO_2	100	<3 min	CO (>1000), ethanol (>20), benzene (>10), acetone (>5)	250
		Benzene	WO_3	1	—	Ethanol (5.8), NH_3 (<1), NO_2 (<1)	301
	Pt & Pd/SiO_2	CH_4	SnO_2	200	—	CO (>1000)	278
	Pt/zeolite MFI	Propane	$SrTi_{0.8}Fe_{0.2}O_{3-\delta}$	500	—	CO (>100), NO (>100), H_2 (>20), propene (>50)	285
		Methanol	Pd/WO_3	2	—	CO (>1000), ethanol (13), acetone (8)	305
	Pd/Al_2O_3, SiO_x, WO_3	CH_4, butane, propane	SnO_x, InO_x	10 000	—	CO, ethanol	51
	Pd/Al_2O_3	CH_4	Pd/SnO_2	50	—	CO (>1000), ethanol (1)	283
			SnO_2	100	<100 ms	CO (10), H_2 (5)	284
	Pd/SnO_2	CO, CH_4	SnO_2	300	—	Ethanol (1)	287
	RuO_2/SiO_2	Propane	SnO_2	150	—	NO_2 (5), CO (2.75)	282
	Mo/zeolite Y	Heptane, octane	$Cr_{1.95}Ti_{0.05}O_3$	—	—	Nonane (1), decane (2), undecane (3)	309
Packed bed	ZnO	Acetone, benzene, H_2, CH_4, toluene	Si/WO_3	0.25	—	Ethanol (81), formaldehyde	294
	Au/$Ce_{0.8}Zr_{0.2}O_2$	CH_4	Pt/SnO_2	5000	35 s	Acetone, CO, ethanol, formaldehyde, toluene (all >100)	288
	Au/Fe_2O_3	CH_4, propane	Pt/SnO_2	2000	10 s	CO, ethanol (both >1000)	291
	Au/TiO_2	Propane	SnO_2	100	—	CO (2.1)	292
	Au/ZnO	Propane	SnO_2	100	—	CO (7.4)	292
	Pt/Al_2O_3	Acetone	Si/WO_3	0.05	55 s	CO (>1000), isoprene (>1000), NH_3 (>1000), ethanol (>500), H_2 (>250)	70
	$Pt/LaFeO_3$	Propane	Pt/SnO_2	1000	30 s	CO (>1), NO (>100)	306

[a] Lowest measured concentration.

Typical catalysts consist of noble metals (*e.g.*, Pt, Pd and Au) on ceramic supports (*e.g.*, Al_2O_3, SiO_2 and Fe_2O_3) that are deposited directly onto sensing films as porous layers. Their working principle is illustrated in Fig. 10a on the example[278] of a SnO_2 sensor (operated at 350 °C) covered by a layer (100–150 μm) of mesoporous Pt/or Pd/SiO_2. Without filter (Fig. 10b), the sensor shows similar resistance changes (*i.e.*, responses) to 20–400 ppm CO (dashed line) and 200–4000 ppm CH_4 (solid line), typical for such SnO_2-based sensors. With filter, CO is fully converted in the filter layer to non-responsive species (*i.e.*, CO_2 and H_2O), while chemically stable CH_4 passes unscathed. As a result (Fig. 10c), no resistance changes to CO are detected anymore, while they are unchanged for CH_4, resulting in selective CH_4 detection.[278] Such CH_4 sensor systems outperform sensors without filter (*e.g.*, methane to CO selectivity of 8 for Pd–Ag activated ZnO[279] and ZnO/ZnO_2 heterostructures[280]) and enabled industrial development of selective gas leak sensors to prevent false alarms.[281]

A variety of catalysts appear suitable for this application, as similar results were obtained with several Al_2O_3- and SiO_x-based catalysts (*e.g.*, thermally evaporated pure Al_2O_3 and SiO_x,[51] drop-coated Pt,[73] Pd[73] and RuO_2[282] on SiO_2,[73] flame deposited Pd/Al_2O_3[283] and screen printed Pt/Al_2O_3,[250] Pd/Al_2O_3[284] and Pt/ZSM-5 zeolites[285]), Ga_2O_3,[286] WO_3,[51] Pd/SnO_2[287] and Au/Ce–Zr.[288] The preferential conversion of VOCs over alkanes is expected due to the alkane's higher chemical stability.[289] Disadvantages of such filters are their limited applicability to alkane detection, as well as typically high operation temperatures (*i.e.*, >350 °C).[278] However, the performance of filters can be improved further and their selectivity tuned more flexibly by exploiting specific analyte–catalyst interactions. For instance, gold catalysts are highly

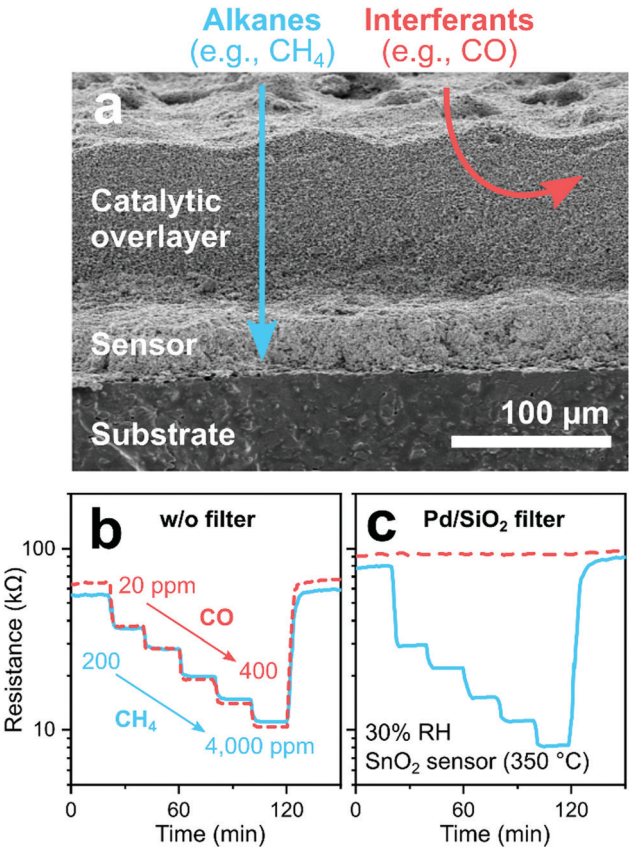

Fig. 10 (a) SEM cross-section of a SnO_2 sensor with a mesoporous catalytic overlayer (filter). Alkanes (*e.g.*, CH_4) pass through the filter unscathed and are detected by the sensor, while interferants (*e.g.*, CO) are converted to non-responsive species (*e.g.*, CO_2). Reproduced with permission.[278] Copyright 2003 Elsevier. SnO_2 sensor response to CO (20–400 ppm, dashed line) and CH_4 (200–4000 ppm, solid line) without (b) and with (c) a Pd/SiO_2 mesoporous catalyst filter at 30% RH.[278]

reactive to CO already at room temperature.[290] In fact, catalytic filters such as Au/Fe_2O_3,[291] Au/ZnO[292] and Au/TiO_2[292] removed CO selectively over alkanes (*e.g.*, propane) even at room temperature, with the highest removal efficiency in the order of Au/Fe_2O_3 > Au/ZnO > Au/TiO_2.

More challenging are filters that distinguish between VOCs with similar stability (*e.g.*, ketones, aldehydes, aromatics), requiring more precise material engineering. For instance, high ethanol background in ambient air or breath (>100 ppm from disinfectants[251] and alcohol consumption,[293] respectively) is a common issue preventing accurate measurements of target analytes. This was addressed by a catalytic filter that exploits surface acidity and basicity (Fig. 11) for selective measurement of acetone,[294] a metabolic breath marker for fat oxidation.[295] The acetone carbonyl group coordinates primarily with Lewis acid sites abundantly present on acidic oxides (*e.g.*, WO_3[296]). In contrast, ethanol conversion is favored on basic oxides featuring surface-adsorbed oxygen- and hydroxyl-related species.[297] Hence, the highest ethanol over acetone selectivity was found for ZnO featuring highest basicity (Fig. 11a–d),[294] in line with literature.[296] Sampling breath of an alcohol intoxicated volunteer through such a small (150 mg) packed bed filter of ZnO heated to 260 °C completely eliminates ethanol interference (Fig. 11e). Most importantly, the filter leaves acetone intact as verified by responses of a Si/WO_3 sensor without and with filter (Fig. 11f) and confirmed by benchtop mass spectrometry. Ethanol responses are strongly reduced (*i.e.*, by 88% at 20 ppm ethanol, remaining response from the combustion to H_2[298]), resulting in selective acetone detection down to 25 ppb in breath-relevant 90% RH with a selectivity to ethanol of 81. This ZnO filter fully combusts also other interferants (*e.g.*, formaldehyde), while leaving aromatics (*e.g.*, toluene, benzene), CH_4 and H_2 intact. The selectivity can be further increased by removing the ethanol conversion products (*i.e.* H_2) by other (catalytic) filters or by operating the filter at higher temperature, although this can reduce the sensitivity by partially converting the target analyte (*i.e.*, acetone).

Catalytic filters can even increase selectivity to analytes from the same chemical group. For instance, the selective detection of carcinogenic[92] benzene over toluene and xylene in indoor air is challenging for chemical gas sensors due to the chemical similarity of these analytes (aromatic hydrocarbons with 0–2 methyl groups).[299] A promising approach is the use of catalytic Co_3O_4 overlayers electron-beam evaporated onto Pd/SnO_2 sensing films.[300] Toluene and *p*-xylene were partially converted in the filter layer to non-reactive species, reducing their responses by as much as 97%, depending on Co_3O_4 thickness (0–60 nm). In contrast, the response to benzene increased by 30% at optimal filter thickness (20 nm), attributed to its activation in the catalytic layer through formation of more responsive intermediates, as has been observed for benzene detection already with Pt/Al_2O_3 filters.[301] As a result, benzene selectivity to *p*-xylene, toluene, ethanol, formaldehyde and CO was doubled from ~1 to >2 that could be further improved with sensors featuring intrinsic benzene selectivity (*e.g.*, Au/multi-walled carbon nanotubes[302] with benzene selectivity towards *o*-xylene and toluene >30). Most interesting, by switching the filter–sensor arrangement, *i.e.*, Co_3O_4 was used as sensor with a catalytic filter layer of SnO_2, also the selectivity could be reversed.[303] Toluene and *p*-xylene responses increased up to a factor of 5 (possibly through formation of more responsive benzyl alcohol[304]), while responses of interferants decreased significantly. As a result, toluene and *p*-xylene selectivity >20 could be achieved towards benzene, ethanol, formaldehyde and CO.

Similarly, increased selectivity through higher sensitivity to target analytes was observed also for other catalytic filters. For instance, a Pd/WO_3 sensor covered by undoped zeolite layers (HZSM-5) increased the CO response by a factor of 7 resulting in selectivity of more than 4 over methanol, ethanol and acetone. Covering the same sensor with Pt/HZSM-5 increased methanol responses by a factor of 15 resulting in selectivity >9 over the same analytes.[305] Packed bed filters of Pt/$LaFeO_3$ heated to 200 °C upstream of Pt/SnO_2 sensors turned them selective to CO with negligible interference from propane.[306] However, when operating the filter at 350 °C, sensor responses to propane increased by a factor of 25 while CO was completely

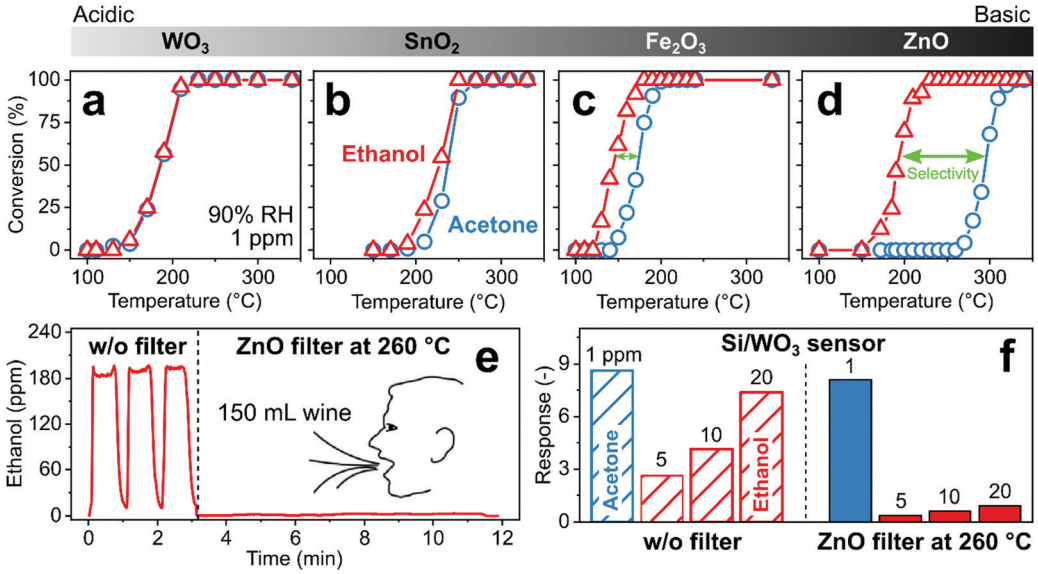

Fig. 11 (a–d) Conversion of 1 ppm ethanol (triangles) and acetone (circles) on metal oxides with increasing basicity, $WO_3 < SnO_2 < Fe_2O_3 < ZnO$, that increases the acetone selectivity over ethanol. (e) Ethanol concentration measured during three consecutive breath exhalations without filter ($t \leq 3$ min) and with 150 mg ZnO filter at 260 °C ($t > 3$ min) that totally eliminated ethanol. (f) Si/WO_3 sensor response to 1 ppm acetone and 5, 10 and 20 ppm ethanol without (open bars) and with a ZnO catalyst at 260 °C (filled bars) upstream of the sensor.[294]

removed. Also, nanolayers (5–20 nm) of Pd or Ag deposited by successive ionic layer deposition on SnO_2 sensors removed ozone interference and increased responses to reducing gases (*e.g.*, CO and H_2).[307] While such catalytic filters offer a powerful tool to enhance sensitivity and tailor selectivity, none of these studies investigated the composition of the effluent, to identify the reformed species and characterize their interaction with the sensor, motivating further research.

Filter configuration

Catalytic filters are typically deposited directly[283] as overlayers (*e.g.*, as porous layers,[283] membranes,[308] zeolites[309] or metallic nanoclusters[310]) onto sensor materials. This results in compact filter–sensor systems where sensing film and catalyst temperature are coupled, requiring no additional heating source. However, this also implies that filter and sensor cannot be fabricated and operated individually to achieve maximum selectivity. Additionally, overlayers may act as diffusion barrier, increasing response times (*e.g.*, from 1 to 4 min for 20–70 μm thick zeolite layers on $SrTi_{1-x}Fe_xO_{3-\delta}$ sensors).[311] While depositing thin[312] or highly porous[278] catalytic overlayers can address this, filter efficiency could be compromised. Finally, solid-state diffusion of the catalytic layer into the sensing film may alter sensor performance (*e.g.*, catalytic Pd diffusion into SnO_2 sensor).[287] This can be solved by an additional inert separation layer (*e.g.*, Al_2O_3[308] or SiO_2[73]).

Such a SnO_2 gas sensor (operated at 375 °C) with a Cr_2O_3 catalytic overlayer deposited by electron-beam evaporation had been tested as ethylene sensor (Fig. 12a–c).[312] Ethylene monitoring is used for controlling growth, development and ripening of fruits.[313] Fig. 12a shows a cross-section SEM image of the Al_2O_3 substrate, the SnO_2 sensing layer (~21 μm) and a thin Cr_2O_3 overlayer (300 nm). Without the Cr_2O_3 overlayer, the SnO_2 sensor features high sensitivity to ethylene, but responds also to trimethylamine (TMA), dimethylamine (DMA), ammonia (NH_3), ethanol, formaldehyde (HCHO) and CO (Fig. 12b). With this catalytic overlayer, the responses to all interfering analytes are reduced, while the ethylene response remains similar. As a result, ethylene selectivity to the tested analytes increases from 1–3.8 to 3.4–24 with an estimated ethylene limit of detection of only 24 ppb. Increasing the Cr_2O_3 layer thickness (from 300 to 600 nm) further reduces responses to interferants but also to ethylene, resulting in overall poorer selectivities. The filter–sensor system was further integrated into a hand-held device with wireless communication, which monitored fruit ripening (exemplarily shown for a banana in Fig. 12c) under controlled conditions (*i.e.*, in a closed chamber). While promising, further validation with a high-resolution instrument (*e.g.*, GC-MS) and testing in indoor air is required.

Catalytic filters can be implemented also as packed beds upstream of the sensor affording individual optimization and operation, as well as flexible combination with different sensors (*e.g.*, chemoresistive, electrochemical or optical). A drawback is the sometimes necessary additional heating source[294] and pressure drop when air is drawn through the filter to the sensor by a pump.[314] The former can be addressed by tailoring materials at the nanoscale (*e.g.*, introducing highly reactive noble metals[290]). Such a compact (30 mg) catalytic packed bed filter of Pt/Al_2O_3 nanoparticles had been used for a selective breath acetone sensor (Fig. 12d–f).[70] Acetone is a breath marker for fat metabolism[295] with applications in personalized exercise[315] and diet monitoring,[316] as well as search and rescue.[317] While Pt/Al_2O_3 is used already to remove VOCs over alkanes, tailoring the Pt-loading is necessary to allow

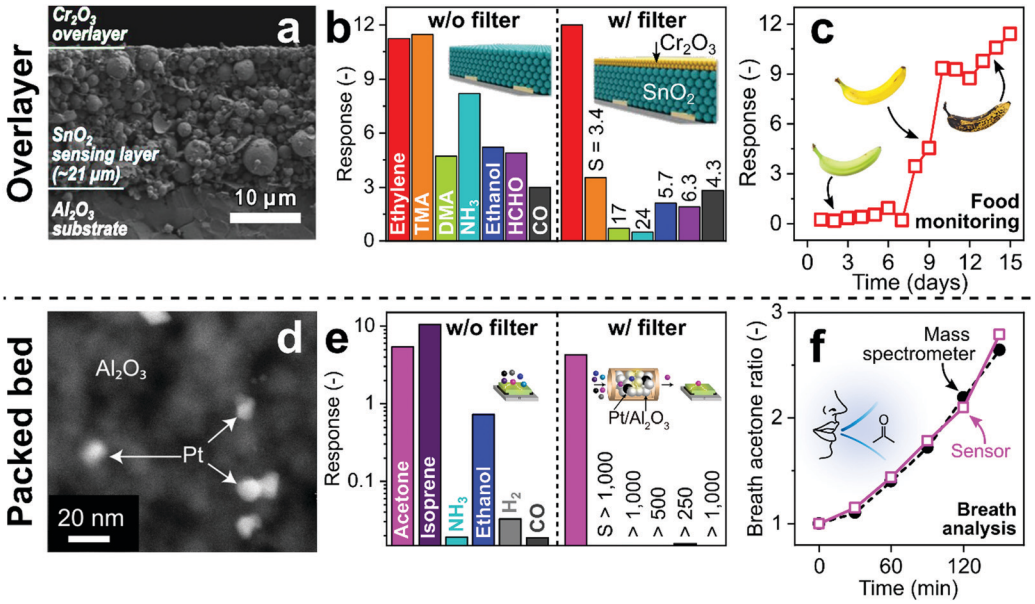

Fig. 12 (a) SnO_2 sensor (375 °C) with catalytic Cr_2O_3 overlayer. Reproduced with permission.[312] Open Access CC BY. (b) SnO_2 sensor response to 2.5 ppm ethylene, trimethylamine (TMA), dimethylamine (DMA), ammonia (NH_3), ethanol, formaldehyde (HCHO) and CO without and with the Cr_2O_3 overlayer with the resulting ethylene selectivties.[312] (c) Sensor response with filter layer when exposed to an underripe ($t < 7$ days), a ripe ($t > 7$ days) and an overripe banana ($t > 10$ days).[312] (d) Catalytic Pt/Al_2O_3 filter. Reproduced with permission.[70] Open Access CC BY. (e) Si/WO_3 sensor (400 °C) response to 1 ppm acetone, isoprene, NH_3, ethanol, H_2 and CO without and with the packed bed Pt/Al_2O_3 filter (135 °C, please note the logarithmic y-axis) resulting in superior acetone selectivity.[70] (f) Breath acetone concentration ratio (normalized to initial concentration) as measured by the Pt/Al_2O_3–Si/WO_3 detector (open squares) and benchtop mass spectrometer (filled circles) during post-exercise rest.[70] Illustrations in (b)[312] and (f)[70] were reproduced with permission. Open Access CC BY.

for selective combustion of breath-relevant interferants over acetone. For example, 0.2 mol% Pt/Al_2O_3 removed selectively isoprene, alcohols, aldehydes, aromatics, CO, H_2 and NH_3 over acetone with high robustness to humidity (30–90% RH) at 135 °C. Fig. 12d shows the crystalline Al_2O_3 particles decorated with 0.2 mol% Pt clusters (average size 9 nm).[70] When coupled to a Si/WO_3 sensor, this results in unprecedented acetone selectivity (>250, Fig. 12e), which cannot be achieved by sensors alone (*e.g.*, selectivity to ethanol <10 by Si/WO_3 and isoprene <4 by Al/ZnO[318]) or orthogonal sensor arrays.[48]

Most importantly, the sensor exhibits sufficiently low limit of detection (*i.e.*, 5.5 ppb that is superior even to 30 ppb by more bulky GC-IMS[319]), and the response time is not affected by the filter (*i.e.*, 1.3 min at 100 ppb). For validation, breath samples after exercise were analyzed by the filter–sensor system and simultaneously with benchtop mass spectrometry (Fig. 12f). The sensor correctly detects the increase of breath acetone indicating fat burning, in excellent agreement with the benchtop method and is applicable also in extreme scenarios (*i.e.*, in presence of alcohol disinfectants as well as >50 ppm H_2 and CH_4 in exhaled breath[320]). Such filter–sensor systems can be implemented readily in commercial and portable breath analyzers.[321]

5. Conclusions and outlook

Today, many commercial sensors already use filters in specific applications (*e.g.*, catalytic and sorption filters in CO[66] and CH_4[67] alarm sensors or GC columns for detection of H_2 and CH_4 in breath[152]). Furthermore, a plethora of next generation sensor technologies and advanced sensing materials are available with impressive performance in the laboratory. To fully assess their potential, they need to be validated under realistic conditions (*e.g.*, detection of pollutants in indoor air[322] or markers in exhaled breath[11]). In fact, today most commercial chemical sensors fail in such emerging applications as they lack the required selectivity.

Filters help single sensors and sensor arrays to overcome selectivity limitations as had been shown already for selective detection of CO[66] and a variety of VOCs (*e.g.*, methanol,[68] isoprene,[71] formaldehyde,[176] trichloroethylene,[167] *etc.*) by sorption filters, H_2[69] and formaldehyde[242] by size-selective filters, and alkanes (*e.g.*, CH_4[67] and propane[292]) and acetone[70] by catalytic filters. Selectivity tuning with filters can be achieved by exploiting a variety of molecular properties of analytes, including molecular size, surface affinity, diffusion properties and chemical reactivity. These are typically not accessible by the sensor alone, which is focused on reactivity (*i.e.*, chemoresistive sensors), electromagnetic absorption (*i.e.*, optical sensors), or molecular mass (*i.e.*, quartz microbalances). By tuning filter selectivity by material design and combination of filters with suitable sensors, an array of new and promising applications is unlocked.

For instance, a handheld methanol detector enabled by a sorption filter can detect methanol-adulteration in drinks,[175] responsible for thousands of victims every year. Such detectors

can also be used to monitor naturally[323] occurring methanol during liquor distillation (*e.g.*, fruit spirit or whisky), detect methanol in the breath of methanol poisoning victims to initiate immediate and appropriate treatment with better chance of recovery,[324] and detect the presence of methanol in sanitizers, responsible for >700 deaths in Iran[325] and USA[326] during the recent COVID-19 pandemic. Even screening for COVID-19 by a quick breath test might be possible after recent research[327] suggested methanol as one of the tentative breath markers of the disease. Or, a sensor enabled by a catalytic filter can selectively detect acetone in the breath.[70] Integrated into a simple-in-use, portable detector, it enables for the first time longitudinal clinical studies with volunteers monitoring their breath acetone independently at home for metabolic profiling. Soon, tracking the effectiveness of different diets (*e.g.*, ketogenic or intermittent fasting) and exercise protocols on fat burn rate or even the non-invasive detection of metabolic diseases might become reality, more important than ever given today's obesity epidemic.[328]

These examples demonstrate how filters drastically increase the selectivity of sensors to meet demanding requirements in emerging applications. This results in useful devices with immediate societal impact. Other examples include sensors for food quality control (*e.g.*, monitoring ethylene during fruit ripening[312]) and air quality monitoring (*e.g.*, fast measurement of formaldehyde in indoor air[176]). Given the immense potential of filters, they will almost certainly play a pivotal role in the future development of advanced sensor systems with unprecedented selectivity as they have done already for CO and CH_4.

Conflicts of interest

The authors report no declarations of interest.

Acknowledgements

This project was supported by the ETH Zurich (Particle Technology Laboratory and Research Grant ETH-05 19-2) and in part the Swiss National Science Foundation (grant 175754 and 170729). Authors are grateful to D. Bischof and F. M. Schenk for helping to design the figures.

References

1 M. Mayer and A. J. Baeumner, *Chem. Rev.*, 2019, **119**, 7996–8027.
2 A. Schütze and T. Sauerwald, in *Advanced Nanomaterials for Inexpensive Gas Microsensors*, ed. E. Llobet, Elsevier, 2020, pp. 209–234.
3 A. C. Rai, P. Kumar, F. Pilla, A. N. Skouloudis, S. Di Sabatino, C. Ratti, A. Yasar and D. Rickerby, *Sci. Total Environ.*, 2017, **607–608**, 691–705.
4 T. Salthammer, S. Mentese and R. Marutzky, *Chem. Rev.*, 2010, **110**, 2536–2572.
5 R. Beelen, G. Hoek, D. Vienneau, M. Eeftens, K. Dimakopoulou, X. Pedeli, M.-Y. Tsai, N. Künzli, T. Schikowski and A. Marcon, *Atmos. Environ.*, 2013, **72**, 10–23.
6 M. Rigby, S. Park, T. Saito, L. Western, A. Redington, X. Fang, S. Henne, A. Manning, R. Prinn and G. Dutton, *Nature*, 2019, **569**, 546–550.
7 H. Yousefi, H.-M. Su, S. M. Imani, K. Alkhaldi, C. D. M. Filipe and T. F. Didar, *ACS Sens.*, 2019, **4**, 808–821.
8 O. L. Gamborg and T. A. LaRue, *Nature*, 1968, **220**, 604–605.
9 C. Lindinger, D. Labbe, P. Pollien, A. Rytz, M. A. Juillerat, C. Yeretzian and I. Blank, *Anal. Chem.*, 2008, **80**, 1574–1581.
10 A. R. Shalaby, *Food Res. Int.*, 1996, **29**, 675–690.
11 A. T. Güntner, S. Abegg, K. Königstein, P. A. Gerber, A. Schmidt-Trucksäss and S. E. Pratsinis, *ACS Sens.*, 2019, **4**, 268–280.
12 S. M. Gordon, J. P. Szidon, B. K. Krotoszynski, R. D. Gibbons and H. J. O'Neill, *Clin. Chem.*, 1985, **31**, 1278–1282.
13 M. J. Henderson, B. Karger and G. Wrenshall, *Diabetes*, 1952, **1**, 188–200.
14 C. N. Tassopoulos, D. Barnett and T. Russell Fraser, *Lancet*, 1969, **293**, 1282–1286.
15 S. T. Senthilmohan, D. B. Milligan, M. J. McEwan, C. G. Freeman and P. F. Wilson, *Redox Rep.*, 2000, **5**, 151–153.
16 S. Giannoukos, A. Agapiou and S. Taylor, *J. Breath Res.*, 2018, **12**, 027106.
17 A. M. Curran, S. I. Rabin, P. A. Prada and K. G. Furton, *J. Chem. Ecol.*, 2005, **31**, 1607–1619.
18 K. E. Jones, K. Dashfield, A. B. Downend and C. M. Otto, *J. Am. Vet. Med. Assoc.*, 2004, **225**, 854–860.
19 B. de Lacy Costello, A. Amann, H. Al-Kateb, C. Flynn, W. Filipiak, T. Khalid, D. Osborne and N. M. Ratcliffe, *J. Breath Res.*, 2014, **8**, 014001.
20 O. O. Hänninen, S. Alm, K. Katsouyanni, N. Künzli, M. Maroni, M. J. Nieuwenhuijsen, K. Saarela, R. J. Srám, D. Zmirou and M. J. Jantunen, *J. Exposure Sci. Environ. Epidemiol.*, 2004, **14**, 440–456.
21 T. Seiyama, A. Kato, K. Fujiishi and M. Nagatani, *Anal. Chem.*, 1962, **34**, 1502–1503.
22 C. Nylander, B. Liedberg and T. Lind, *Sens. Actuators*, 1982, **3**, 79–88.
23 N. J. Pineau, S. D. Keller, A. T. Güntner and S. E. Pratsinis, *Microchim. Acta*, 2020, **187**, 96.
24 M. E. Prévôt, A. Nemati, T. R. Cull, E. Hegmann and T. Hegmann, *Adv. Mater. Technol.*, 2020, **5**, 2000058.
25 L. Wang, A. Teleki, S. E. Pratsinis and P. I. Gouma, *Chem. Mater.*, 2008, **20**, 4794–4796.
26 V. Jayaraman, G. Mangamma, T. Gnanasekaran and G. Periaswami, *Solid State Ionics*, 1996, **86**, 1111–1114.
27 T. Ishihara, K. Shiokawa, K. Eguchi and H. Arai, *Chem. Lett.*, 1988, 997–1000.
28 H.-J. Cho, Y. H. Kim, S. Park and I.-D. Kim, *ChemNanoMat*, 2020, **6**, 1014–1027.
29 Z. Dai, T. Liang and J.-H. Lee, *Nanoscale Adv.*, 2019, **1**, 1626–1639.

30 J. A. Kemmler, S. Pokhrel, J. Birkenstock, M. Schowalter, A. Rosenauer, N. Barsan, U. Weimar and L. Mädler, *Sens. Actuators, B*, 2012, **161**, 740–747.
31 A. T. Güntner, N. J. Pineau, D. Chie, F. Krumeich and S. E. Pratsinis, *J. Mater. Chem. B*, 2016, **4**, 5358–5366.
32 A. T. Güntner, M. Righettoni and S. E. Pratsinis, *Sens. Actuators, B*, 2016, **223**, 266–273.
33 R. Qian, Z. Yumin, L. Tianping, S. Kaiyuan, Z. Baoye, Z. Zhongqi, Z. Jin and L. Qingju, *Nanotechnology*, 2018, **29**, 145503.
34 M. Bendahan, C. Jacolin, P. Lauque, J.-L. Seguin and P. Knauth, *J. Phys. Chem. B*, 2001, **105**, 8327–8333.
35 M. Akiyama, J. Tamaki, N. Miura and N. Yamazoe, *Chem. Lett.*, 1991, 1611–1614.
36 M. Hauptmann, P. A. Stewart, J. H. Lubin, L. E. Beane Freeman, R. W. Hornung, R. F. Herrick, R. N. Hoover, J. F. Fraumeni Jr, A. Blair and R. B. Hayes, *J. Natl. Cancer Inst.*, 2009, **101**, 1696–1708.
37 C. J. Weschler, *Indoor Air*, 2000, **10**, 269–288.
38 K. Persaud and G. Dodd, *Nature*, 1982, **299**, 352–355.
39 W. Hu, L. Wan, Y. Jian, C. Ren, K. Jin, X. Su, X. Bai, H. Haick, M. Yao and W. Wu, *Adv. Mater. Technol.*, 2019, **4**, 1800488.
40 A. Hierlemann and R. Gutierrez-Osuna, *Chem. Rev.*, 2008, **108**, 563–613.
41 S. Matindoust, M. Baghaei-Nejad, M. H. S. Abadi, Z. Zou and L.-R. Zheng, *Sens. Rev.*, 2016, **36**, 169–183.
42 R. E. Amor, M. K. Nakhleh, O. Barash and H. Haick, *Eur. Respir. Rev.*, 2019, **28**, 190002.
43 S. Haykin and K. R. Liu, *Handbook on array processing and sensor networks*, John Wiley & Sons, 2010.
44 Z. Chen, Z. Chen, Z. Song, W. Ye and Z. Fan, *J. Semicond.*, 2019, **40**, 111601.
45 G. Peng, U. Tisch, O. Adams, M. Hakim, N. Shehada, Y. Y. Broza, S. Billan, R. Abdah-Bortnyak, A. Kuten and H. Haick, *Nat. Nanotechnol.*, 2009, **4**, 669–673.
46 M. B. Banerjee, R. B. Roy, B. Tudu, R. Bandyopadhyay and N. Bhattacharyya, *J. Food Eng.*, 2019, **244**, 55–63.
47 F. Röck, N. Barsan and U. Weimar, *Chem. Rev.*, 2008, **108**, 705–725.
48 N. J. Pineau, J. F. Kompalla, A. T. Güntner and S. E. Pratsinis, *Microchim. Acta*, 2018, **185**, 563.
49 S. R. Morrison, *Sens. Actuators*, 1987, **12**, 425–440.
50 G. Korotcenkov, *Handbook of Gas Sensor Materials: Properties, Advantages and Shortcomings for Applications Volume 1: Conventional Approaches*, Springer New York, New York, NY, 2013, pp. 293–303.
51 C. A. Papadopoulos, D. S. Vlachos and J. N. Avaritsiotis, *Sens. Actuators, B*, 1996, **32**, 61–69.
52 F. Röck, N. Barsan and U. Weimar, *Chem. Rev.*, 2008, **108**, 705–725.
53 K. Sahner, G. Hagen, D. Schonauer, S. Reiss and R. Moos, *Solid State Ionics*, 2008, **179**, 2416–2423.
54 W.-T. Koo, J.-S. Jang and I.-D. Kim, *Chem*, 2019, **5**, 1938–1963.
55 T. Wagner, S. Haffer, C. Weinberger, D. Klaus and M. Tiemann, *Chem. Soc. Rev.*, 2013, **42**, 4036–4053.
56 C. Allman and G. Khilnani, *Adv. Instrum.*, 1983, **38**, 399–406.
57 A. Ryzhikov, M. Labeau and A. Gaskov, *Selectivity Improvement of Semiconductor Gas Sensors by Filters*, presented in part at the Sensors for Environment, Health and Security, Dordrecht, 2009.
58 D. J. Wales, J. Grand, V. P. Ting, R. D. Burke, K. J. Edler, C. R. Bowen, S. Mintova and A. D. Burrows, *Chem. Soc. Rev.*, 2015, **44**, 4290–4321.
59 J. B. Miller, *IEEE Sens. J.*, 2001, **1**, 88–93.
60 C. Pijolat, B. Riviere, M. Kamionka, J. P. Viricelle and P. Breuil, *J. Mater. Sci.*, 2003, **38**, 4333–4346.
61 J.-W. Yoon and J.-H. Lee, *Lab Chip*, 2017, **17**, 3537–3557.
62 G. N. Advani and A. G. Jordan, *J. Electron. Mater.*, 1980, **9**, 29–49.
63 K. Fukui and K. Komatsu, Proceedings of the International Meeting on Chemical Sensors, Analytical Chemistry Symposia Series, Fukuoka, Japan, 1983, vol. 17, pp. 52–36.
64 S. J. Gentry and S. R. Howarth, *Sens. Actuators*, 1984, **5**, 265–273.
65 K. Nagashima and S. Suzuki, *Anal. Chim. Acta*, 1984, **162**, 153–159.
66 M. Schweizer-Berberich, S. Strathmann, W. Göpel, R. Sharma and A. Peyre-Lavigne, *Sens. Actuators, B*, 2000, **66**, 34–36.
67 H. Debéda, P. Massok, C. Lucat, F. Ménil and J.-L. Aucouturier, *Meas. Sci. Technol.*, 1997, **8**, 99–110.
68 J. van den Broek, S. Abegg, S. E. Pratsinis and A. T. Güntner, *Nat. Commun.*, 2019, **10**, 4220.
69 F. A. A. Nugroho, I. Darmadi, L. Cusinato, A. Susarrey-Arce, H. Schreuders, L. J. Bannenberg, A. B. da Silva Fanta, S. Kadkhodazadeh, J. B. Wagner, T. J. Antosiewicz, A. Hellman, V. P. Zhdanov, B. Dam and C. Langhammer, *Nat. Mater.*, 2019, **18**, 489–495.
70 I. C. Weber, H. P. Braun, F. Krumeich, A. T. Güntner and S. E. Pratsinis, *Adv. Sci.*, 2020, **7**, 2001503.
71 J. van den Broek, A. T. Güntner and S. E. Pratsinis, *ACS Sens.*, 2018, **3**, 677–683.
72 Y. Li, J. Liu, M. Liu, F. Yu, L. Zhang, H. Tang, B.-C. Ye and L. Lai, *Electrochem. Commun.*, 2016, **64**, 42–45.
73 C. H. Kwon, D. H. Yun, H.-K. Hong, S.-R. Kim, K. Lee, H. Y. Lim and K. H. Yoon, *Sens. Actuators, B*, 2000, **65**, 327–330.
74 R. T. Yang, *Gas separation by adsorption processes*, Butterworth-Heinemann, 2013.
75 O. Hugon, M. Sauvan, P. Benech, C. Pijolat and F. Lefebvre, *Sens. Actuators, B*, 2000, **67**, 235–243.
76 T. Oyabu, Y. Matuura and R. Murai, *Sens. Actuators, B*, 1990, **1**, 218–221.
77 X. Zhang, B. Gao, A. E. Creamer, C. Cao and Y. Li, *J. Hazard. Mater.*, 2017, **338**, 102–123.
78 S. Brunauer, L. S. Deming, W. E. Deming and E. Teller, *J. Am. Chem. Soc.*, 1940, **62**, 1723–1732.
79 S. J. Gregg, K. S. W. Sing and H. Salzberg, *J. Electrochem. Soc.*, 1967, **114**, 279C.
80 Scientific Instrument Services (SIS), Tenax® TA breakthrough volume data, https://www.sisweb.com/index/referenc/tenaxta.htm, (accessed 2019/08/20).

81 M. Harper, *J. Chromatogr. A*, 2000, **885**, 129–151.
82 J. Rouquerol, F. Rouquerol, P. Llewellyn, G. Maurin and K. S. Sing, *Adsorption by powders and porous solids: principles, methodology and applications*, Academic Press, 2013.
83 I. M. Klotz, *Chem. Rev.*, 1946, **39**, 241–268.
84 N. Mohan, G. K. Kannan, S. Upendra, R. Subha and N. S. Kumar, *J. Hazard. Mater.*, 2009, **168**, 777–781.
85 M. Harper, *Ann. Occup. Hyg.*, 1993, **37**, 65–88.
86 Z.-H. Huang, F. Kang, K.-M. Liang and J. Hao, *J. Hazard. Mater.*, 2003, **98**, 107–115.
87 K. Frank, H. Kohler and U. Guth, *Sens. Actuators, B*, 2009, **141**, 361–369.
88 K. Allen, T. Von Backström and D. Kröger, *Powder Technol.*, 2013, **246**, 590–600.
89 K. Dettmer and W. Engewald, *Anal. Bioanal. Chem.*, 2002, **373**, 490–500.
90 R. J. Peters and H. A. Bakkeren, *Analyst*, 1994, **119**, 71–74.
91 C. Turner, P. Španěl and D. Smith, *Physiol. Meas.*, 2006, **27**, 321–337.
92 World Health Organization, WHO guidelines for indoor air quality: selected pollutants, 2010.
93 K.-D. Kwon, W.-K. Jo, H.-J. Lim and W.-S. Jeong, *J. Hazard. Mater.*, 2007, **148**, 192–198.
94 F. Gritti and G. Guiochon, *Anal. Chem.*, 2006, **78**, 4642–4653.
95 D. S. Hage, *Principles and Applications of Clinical Mass Spectrometry*, Elsevier, 2018.
96 L. Ferrus, H. Guenard, G. Vardon and P. Varene, *Respir. Physiol.*, 1980, **39**, 367–381.
97 I. Maier and M. Fieber, *J. High Resolut. Chromatogr.*, 1988, **11**, 566–576.
98 G. Odell Wood, *Carbon*, 1992, **30**, 593–599.
99 A. A. Pesaran and A. F. Mills, *Int. J. Heat Mass Transfer*, 1987, **30**, 1037–1049.
100 X. Zhao, Q. Ma and G. Lu, *Energy Fuels*, 1998, **12**, 1051–1054.
101 K. Sakodynskii, L. Panina and N. Klinskaya, *Chromatographia*, 1974, **7**, 339–344.
102 A. Khaleel, P. N. Kapoor and K. J. Klabunde, *Nanostruct. Mater.*, 1999, **11**, 459–468.
103 S. Brosillon, M.-H. Manero and J.-N. Foussard, *Environ. Sci. Technol.*, 2001, **35**, 3571–3575.
104 N. M. Padial, E. Quartapelle Procopio, C. Montoro, E. López, J. E. Oltra, V. Colombo, A. Maspero, N. Masciocchi, S. Galli and I. Senkovska, *Angew. Chem., Int. Ed.*, 2013, **52**, 8290–8294.
105 O. K. Farha, I. Eryazici, N. C. Jeong, B. G. Hauser, C. E. Wilmer, A. A. Sarjeant, R. Q. Snurr, S. T. Nguyen, A. Ö. Yazaydın and J. T. Hupp, *J. Am. Chem. Soc.*, 2012, **134**, 15016–15021.
106 J. Rouquerol, D. Avnir, C. Fairbridge, D. Everett, J. Haynes, N. Pernicone, J. Ramsay, K. Sing and K. Unger, *Pure Appl. Chem.*, 1994, **66**, 1739–1758.
107 C. Baerlocher, L. B. McCusker and D. H. Olson, *Atlas of zeolite framework types*, Elsevier, 2007.
108 T. G. Glover and B. Mu, *Gas Adsorption in Metal-Organic Frameworks: Fundamentals and Applications*, CRC Press, 2018.
109 J.-M. Li and O. Talu, in *Studies in Surface Science and Catalysis*, ed. M. Suzuki, Elsevier, 1993, vol. 80, pp. 373–380.
110 K. Yang, Q. Sun, F. Xue and D. Lin, *J. Hazard. Mater.*, 2011, **195**, 124–131.
111 Y. Morigami, M. Kondo, J. Abe, H. Kita and K. Okamoto, *Sep. Purif. Technol.*, 2001, **25**, 251–260.
112 Y. Sun, B. Gao, Y. Yao, J. Fang, M. Zhang, Y. Zhou, H. Chen and L. Yang, *Chem. Eng. J.*, 2014, **240**, 574–578.
113 W. Shen, Z. Li and Y. Liu, *Recent Pat. Chem. Eng.*, 2008, **1**, 27–40.
114 L. Li, S. Liu and J. Liu, *J. Hazard. Mater.*, 2011, **192**, 683–690.
115 J. Boudou, A. Martinez-Alonzo and J. Tascon, *Carbon*, 2000, **38**, 1021–1029.
116 C. L. Mangun, K. R. Benak, J. Economy and K. L. Foster, *Carbon*, 2001, **39**, 1809–1820.
117 J. L. Figueiredo, M. Pereira, M. Freitas and J. Orfao, *Carbon*, 1999, **37**, 1379–1389.
118 L. Lalhmunsiama, S. M. Lee, S. S. Choi and D. Tiwari, *Metals*, 2017, **7**, 248.
119 Y. Li, J. He, Z. Kaisheng, T. Liu, Y. Hu, X. Chen, X. Huang, L. Kong and J. Liu, *RSC Adv.*, 2019, **9**, 397–407.
120 S. Dipendu and D. Shuguang, *Tsinghua Sci. Technol.*, 2010, **15**, 363–376.
121 A. Stone, *The theory of intermolecular forces*, Oxford University Press, 2013.
122 H.-J. Butt and M. Kappl, *Surface and interfacial forces*, Wiley Online Library, 2010.
123 G. A. Jeffrey, *An introduction to hydrogen bonding*, Oxford University Press, 1997.
124 S. Sircar, M. B. Rao and T. C. Golden, in *Studies in Surface Science and Catalysis*, ed. A. Dąbrowski and V. A. Tertykh, Elsevier, 1996, vol. 99, pp. 629–646.
125 M. Nishibori, W. Shin, N. Izu, T. Itoh and I. Matsubara, *Sens. Actuators, B*, 2009, **137**, 524–528.
126 H. Suto and G. Inoue, *J. Atmos. Ocean. Technol.*, 2010, **27**, 1175–1184.
127 Ł. Guz, G. Łagód, K. Jaromin-Gleń, Z. Suchorab, H. Sobczuk and A. Bieganowski, *Sensors*, 2015, **15**, 1–21.
128 D. Vlachos, P. Skafidas and J. Avaritsiotis, *Sens. Actuators, B*, 1995, **25**, 491–494.
129 A. Prabhakar, R. A. Iglesias, X. Shan, X. Xian, L. Zhang, F. Tsow, E. S. Forzani and N. Tao, *Anal. Chem.*, 2012, **84**, 7172–7178.
130 L.-Y. Chang, M.-Y. Chuang, H.-W. Zan, H.-F. Meng, C.-J. Lu, P.-H. Yeh and J.-N. Chen, *ACS Sens.*, 2017, **2**, 531–539.
131 N. Yamazoe, J. Fuchigami, M. Kishikawa and T. Seiyama, *Surf. Sci.*, 1979, **86**, 335–344.
132 R. H. Castro and D. V. Quach, *J. Phys. Chem. C*, 2012, **116**, 24726–24733.
133 R. Salerno-Kennedy and K. D. Cashman, *Wien. Klin. Wochenschr.*, 2005, **117**, 180–186.
134 M. Schweizer-Berberich, S. Strathmann, U. Weimar, R. Sharma, A. Seube, A. Peyre-Lavigne and W. Göpel, *Sens. Actuators, B*, 1999, **58**, 318–324.

135 M. Righettoni, A. Tricoli, S. Gass, A. Schmid, A. Amann and S. E. Pratsinis, *Anal. Chim. Acta*, 2012, **738**, 69–75.
136 S. Schon, S. J. Theodore and A. T. Güntner, *Sens. Actuators, B*, 2018, **273**, 1780–1785.
137 A. Teleki, S. E. Pratsinis, K. Kalyanasundaram and P. I. Gouma, *Sens. Actuators, B*, 2006, **119**, 683–690.
138 A. T. Güntner, V. Koren, K. Chikkadi, M. Righettoni and S. E. Pratsinis, *ACS Sens.*, 2016, **1**, 528–535.
139 P.-I. Gouma, L. Wang, S. R. Simon and M. Stanacevic, *Sensors*, 2017, **17**, 199.
140 L. Cisneros, F. Gao and A. Corma, *Microporous Mesoporous Mater.*, 2019, **283**, 25–30.
141 R. L. Jordan, C. P. Hauser and A. G. Dawson, *Analyst*, 1997, **122**, 811–814.
142 G. Bergshoeff, R. W. Lanting, J. van Ham, J. M. Prop and H. F. Reijnders, *Analyst*, 1984, **109**, 1165–1169.
143 W. R. Penrose, L. Pan, J. R. Stetter and W. M. Ollison, *Anal. Chim. Acta*, 1995, **313**, 209–219.
144 J. Brunet, L. Spinelle, A. Pauly, M. Dubois, K. Guerin, M. Bouvet, C. Varenne, B. Lauron and A. Hamwi, *Org. Electron.*, 2010, **11**, 1223–1229.
145 J. Brunet, A. Pauly, M. Dubois, M. L. Rodriguez-Mendez, A. L. Ndiaye, C. Varenne and K. Guérin, *Talanta*, 2014, **127**, 100–107.
146 G. A. Lawrance, *Introduction to coordination chemistry*, John Wiley & Sons, 2013.
147 A. I. Popov and W. W. Wendlandt, *J. Am. Chem. Soc.*, 1955, **77**, 857–859.
148 A. T. Güntner, M. Wied, N. J. Pineau and S. E. Pratsinis, *Adv. Sci.*, 2020, **7**, 1903390.
149 N. J. Pineau, F. Krumeich, A. T. Güntner and S. E. Pratsinis, *Sens. Actuators, B*, 2021, **327**, 128843.
150 H. M. McNair, J. M. Miller and N. H. Snow, *Basic gas chromatography*, John Wiley & Sons, 2019.
151 B. P. Regmi and M. Agah, *Anal. Chem.*, 2018, **90**, 13133–13150.
152 Quintron, BreathTracker Analyzer, https://www.breathtests.com/instrumentation, (accessed 2020/06/02).
153 M. Li, E. B. Myers, H. X. Tang, S. J. Aldridge, H. C. McCaig, J. J. Whiting, R. J. Simonson, N. S. Lewis and M. L. Roukes, *Nano Lett.*, 2010, **10**, 3899–3903.
154 S. C. Terry, J. H. Jerman and J. B. Angell, *IEEE Trans. Electron Devices*, 1979, **26**, 1880–1886.
155 H. Zhu, J. She, M. Zhou and X. Fan, *Sens. Actuators, B*, 2019, **283**, 182–187.
156 H. Jung, W. Cho, R. Yoo, H.-S. Lee, Y.-S. Choe, J. Y. Jeon and W. Lee, *Sens. Actuators, B*, 2018, **274**, 527–532.
157 M. Zhou, J. Lee, H. Zhu, R. Nidetz, K. Kurabayashi and X. Fan, *RSC Adv.*, 2016, **6**, 49416–49424.
158 F. Gao, M. Wang, X. Zhang, J. Zhang, Y. Xue, H. Wan and P. Wang, *Anal. Methods*, 2018, **10**, 4329–4338.
159 H. Meng, W. Yang, X. Yan, Y. Zhang, L. Feng and Y. Guan, *Sens. Actuators, B*, 2015, **216**, 511–517.
160 I. Lara-lbeas, A. Rodríguez-Cuevas, C. Andrikopoulou, V. Person, L. Baldas, S. Colin and S. Le Calvé, *Micromachines*, 2019, **10**, 187.
161 K. M. Skog, F. Xiong, H. Kawashima, E. Doyle, R. Soto and D. R. Gentner, *Anal. Chem.*, 2019, **91**, 1318–1327.
162 J. Lee, M. Zhou, H. Zhu, R. Nidetz, K. Kurabayashi and X. Fan, *Anal. Chem.*, 2016, **88**, 10266–10274.
163 J. Lee, S. K. Sayler, M. Zhou, H. Zhu, R. J. Richardson, R. L. Neitzel, K. Kurabayashi and X. Fan, *Anal. Methods*, 2018, **10**, 237–244.
164 Defiant Technologies, TOCAM, https://www.defiant-tech.com/tocam-portable-gas-chromatograph-gc/, (accessed 2020/06/03).
165 Dräger, X-pid 9000/9500, https://www.draeger.com/en_seeur/Applications/Products/Portable-Gas-Detection/Multi-Gas-Detectors/X-pid-9000-9500, (accessed 2020/06/03).
166 S. Zampolli, I. Elmi, G. C. Cardinali, L. Masini, F. Bonafè and F. Zardi, *Sens. Actuators, B*, 2020, **305**, 127444.
167 J. Wang, N. Nuñovero, R. Nidetz, S. J. Peterson, B. M. Brookover, W. H. Steinecker and E. T. Zellers, *Anal. Chem.*, 2019, **91**, 4747–4754.
168 Y. Qin and Y. B. Gianchandani, *Microsyst. Nanoeng.*, 2016, **2**, 15049.
169 T. Tzeng, C. Kuo, S. Wang, P. Huang, Y. Huang, W. Hsieh, Y. Huang, P. Kuo, S. Yu, S. Lee, Y. J. Tseng, W. Tian and S. Lu, *IEEE J. Solid-State Circuits*, 2016, **51**, 259–272.
170 P. R. Lewis, P. Manginell, D. R. Adkins, R. J. Kottenstette, D. R. Wheeler, S. S. Sokolowski, D. E. Trudell, J. E. Byrnes, M. Okandan, J. M. Bauer, R. G. Manley and C. Frye-Mason, *IEEE Sens. J.*, 2006, **6**, 784–795.
171 S. Zampolli, I. Elmi, F. Mancarella, P. Betti, E. Dalcanale, G. C. Cardinali and M. Severi, *Sens. Actuators, B*, 2009, **141**, 322–328.
172 S. K. Kim, H. Chang and E. T. Zellers, *Anal. Chem.*, 2011, **83**, 7198–7206.
173 W. R. Collin, G. Serrano, L. K. Wright, H. Chang, N. Nuñovero and E. T. Zellers, *Anal. Chem.*, 2014, **86**, 655–663.
174 J. Wang, J. Bryant-Genevier, N. Nuñovero, C. Zhang, B. Kraay, C. Zhan, K. Scholten, R. Nidetz, S. Buggaveeti and E. T. Zellers, *Microsyst. Nanoeng.*, 2018, **4**, 17101.
175 S. Abegg, L. Magro, J. van den Broek, S. E. Pratsinis and A. T. Güntner, *Nat. Food*, 2020, **1**, 351–354.
176 J. van den Broek, D. K. Cerrejon, S. E. Pratsinis and A. T. Güntner, *J. Hazard. Mater.*, 2020, **399**, 123052.
177 H. L. Tian, H. Q. Fan, M. M. Li and L. T. Ma, *ACS Sens.*, 2016, **1**, 243–250.
178 D. Meng, D. Liu, G. Wang, Y. Shen, X. San, M. Li and F. Meng, *Sens. Actuators, B*, 2018, **273**, 418–428.
179 IUPAC, *Compendium of Chemical Terminology*, Blackwell Scientific Publications, 2019.
180 R. Barro, J. Regueiro, M. Llompart and C. Garcia-Jares, *J. Chromatogr. A*, 2009, **1216**, 540–566.
181 T. T. Zhou, Y. T. Sang, X. X. Wang, C. Y. Wu, D. W. Zeng and C. S. Xie, *Sens. Actuators, B*, 2018, **258**, 1099–1106.
182 N. Kosinov, C. Auffret, C. Gücüyener, B. M. Szyja, J. Gascon, F. Kapteijn and E. J. M. Hensen, *J. Mater. Chem. A*, 2014, **2**, 13083–13092.
183 H. Li, Z. Song, X. Zhang, Y. Huang, S. Li, Y. Mao, H. J. Ploehn, Y. Bao and M. Yu, *Science*, 2013, **342**, 95–98.

184 N. Kosinov, J. Gascon, F. Kapteijn and E. J. M. Hensen, *J. Membr. Sci.*, 2016, **499**, 65–79.
185 S. M. Auerbach, K. A. Carrado and P. K. Dutta, *Handbook of zeolite science and technology*, CRC Press, 2003.
186 S. Qiu, M. Xue and G. Zhu, *Chem. Soc. Rev.*, 2014, **43**, 6116–6140.
187 S.-Y. Ding and W. Wang, *Chem. Soc. Rev.*, 2013, **42**, 548–568.
188 M. A. Ruiz, A. Sua and F. Tian, in *Encyclopedia of Interfacial Chemistry*, ed. K. Wandelt, Elsevier, Oxford, 2018, pp. 646–671.
189 J. Liang, Z. Liang, R. Zou and Y. Zhao, *Adv. Mater.*, 2017, **29**, 1701139.
190 T. F. Degnan Jr, C. M. Smith and C. R. Venkat, *Appl. Catal., A*, 2001, **221**, 283–294.
191 R. E. Morris and P. S. Wheatley, *Angew. Chem., Int. Ed.*, 2008, **47**, 4966–4981.
192 S. S.-Y. Chui, S. M.-F. Lo, J. P. H. Charmant, A. G. Orpen and I. D. Williams, *Science*, 1999, **283**, 1148–1150.
193 J. Zhang, Y. Tan and W.-J. Song, *Microchim. Acta*, 2020, **187**, 234.
194 A. F. Ismail, K. C. Khulbe and T. Matsuura, *Gas separation membranes*, Springer, 2015.
195 R. Krishna and J. Wesselingh, *Chem. Eng. Sci.*, 1997, **52**, 861–911.
196 Z. Kang, L. Fan and D. Sun, *J. Mater. Chem. A*, 2017, **5**, 10073–10091.
197 C. Chi, X. Wang, Y. Peng, Y. Qian, Z. Hu, J. Dong and D. Zhao, *Chem. Mater.*, 2016, **28**, 2921–2927.
198 P. S. Goh, A. F. Ismail, S. M. Sanip, B. C. Ng and M. Aziz, *Sep. Purif. Technol.*, 2011, **81**, 243–264.
199 C. D. Feng, *J. Electrochem. Soc.*, 1994, **141**, 220–225.
200 M. Fleischer, M. Seth, C. D. Kohl and H. Meixner, *Sens. Actuators, B*, 1996, **36**, 297–302.
201 J. Goschnick, M. Frietsch and T. Schneider, *Surf. Coat. Technol.*, 1998, **108–109**, 292–296.
202 Z. L. Zhan, D. G. Jiang and J. Q. Xu, *Mater. Chem. Phys.*, 2005, **90**, 250–254.
203 A. Katsuki and K. Fukui, *Sens. Actuators, B*, 1998, **52**, 30–37.
204 X. Meng, Q. Zhang, S. Zhang and Z. He, *Sensors*, 2019, **19**, 2478.
205 J. Hu, Y. Sun, Y. Xue, M. Zhang, P. Li, K. Lian, S. Zhuiykov, W. Zhang and Y. Chen, *Sens. Actuators, B*, 2018, **257**, 124–135.
206 W. J. Buttner, M. B. Post, R. Burgess and C. Rivkin, *Int. J. Hydrogen Energy*, 2011, **36**, 2462–2470.
207 Y. Luo, C. Zhang, B. Zheng, X. Geng and M. Debliquy, *Int. J. Hydrogen Energy*, 2017, **42**, 20386–20397.
208 K. Wada and M. Egashira, *Sens. Actuators, B*, 2000, **62**, 211–219.
209 G. Tournier and C. Pijolat, *Sens. Actuators, B*, 2005, **106**, 553–562.
210 US Department of Energy, Hydrogen, Fuel Cells and Infrastructure Technologies Program: Multi-Year Research, Development and Demonstration Plan, 2007.
211 V. V. Sysoev, I. Kiselev, V. Trouillet and M. Bruns, *Sens. Actuators, B*, 2013, **185**, 59–69.
212 S. Ehrmann, J. Jüngst, J. Goschnick and D. Everhard, *Sens. Actuators, B*, 2000, **65**, 247–249.
213 C. Arnold, M. Harms and J. Goschnick, *IEEE Sens. J.*, 2002, **2**, 179–188.
214 N. Kodakari, T. Sakamoto, K. Shinkawa, H. Funabiki, N. Katada and M. Niwa, *Bull. Chem. Soc. Jpn.*, 1998, **71**, 513–519.
215 M. Sekiyama, N. Katada and M. Niwa, *Sens. Actuators, B*, 2007, **124**, 398–406.
216 L. Huang, M. Zhang, C. Li and G. Shi, *J. Phys. Chem. Lett.*, 2015, **6**, 2806–2815.
217 S. C. O'Hern, M. S. Boutilier, J.-C. Idrobo, Y. Song, J. Kong, T. Laoui, M. Atieh and R. Karnik, *Nano Lett.*, 2014, **14**, 1234–1241.
218 J. Zhao, G. He, S. Huang, L. F. Villalobos, M. Dakhchoune, H. Bassas and K. V. Agrawal, *Sci. Adv.*, 2019, **5**, eaav1851.
219 J. S. Jarig, J. Lee, W. T. Koo, D. H. Kim, H. J. Cho, H. Shin and I. D. Kim, *Anal. Chem.*, 2020, **92**, 957–965.
220 M. Drobek, J. H. Kim, M. Bechelany, C. Vallicari, A. Julbe and S. S. Kim, *ACS Appl. Mater. Interfaces*, 2016, **8**, 8323–8328.
221 M. Chi and Y.-P. Zhao, *Comput. Mater. Sci.*, 2009, **46**, 1085–1090.
222 Z. Li, N. Wang, Z. Lin, J. Wang, W. Liu, K. Sun, Y. Q. Fu and Z. Wang, *ACS Appl. Mater. Interfaces*, 2016, **8**, 20962–20968.
223 M. Vilaseca, J. Coronas, A. Cirera, A. Cornet, J. R. Morante and J. Santamaria, *Sens. Actuators, B*, 2007, **124**, 99–110.
224 G. Lu and J. T. Hupp, *J. Am. Chem. Soc.*, 2010, **132**, 7832–7833.
225 A. Lan, K. Li, H. Wu, D. H. Olson, T. J. Emge, W. Ki, M. Hong and J. Li, *Angew. Chem., Int. Ed.*, 2009, **48**, 2334–2338.
226 H. Bux, F. Liang, Y. Li, J. Cravillon, M. Wiebcke and J. Caro, *J. Am. Chem. Soc.*, 2009, **131**, 16000–16001.
227 X. N. Wu, S. S. Xiong, Z. H. Mao, S. Hu and X. G. Long, *Chem. – Eur. J.*, 2017, **23**, 7969–7975.
228 M. Weber, J. H. Kim, J. H. Lee, J. Y. Kim, I. Iatsunskyi, E. Coy, M. Drobek, A. Julbe, M. Bechelany and S. S. Kim, *ACS Appl. Mater. Interfaces*, 2018, **10**, 34765–34773.
229 C. Wadell, S. Syrenova and C. Langhammer, *ACS Nano*, 2014, **8**, 11925–11940.
230 Y. Zhou, T. Zhou, Y. Zhang, L. Tang, Q. Guo, M. Wang, C. Xie and D. Zeng, *Solid State Ionics*, 2020, **350**, 115278.
231 Z. Qiao, Q. Xu and J. Jiang, *J. Mater. Chem. A*, 2018, **6**, 18898–18905.
232 K. B. Sezginel, S. Keskin and A. Uzun, *Langmuir*, 2016, **32**, 1139–1147.
233 K. S. Walton, M. B. Abney and M. D. LeVan, *Microporous Mesoporous Mater.*, 2006, **91**, 78–84.
234 T. Zhou, Z. Qin, X. Wang, C. Wu, X. Tang, T. Zhang, H. Wang, C. Xie and D. Zeng, *Chem. Commun.*, 2019, **55**, 11045–11048.
235 M. Vilaseca, J. Coronas, A. Cirera, A. Cornet, J. R. Morante and J. Santamaría, *Catal. Today*, 2003, **82**, 179–185.
236 M. Vilaseca, J. Coronas, A. Cirera, A. Cornet, J. Morante and J. Santamaria, *Sens. Actuators, B*, 2008, **133**, 435–441.

237 K. Fukui and S. Nishida, *Sens. Actuators, B*, 1997, **45**, 101–106.
238 R. Binions, H. Davies, A. Afonja, S. Dungey, D. Lewis, D. E. Williams and I. P. Parkin, *J. Electrochem. Soc.*, 2009, **156**, J46–J51.
239 S. Galioglu, I. Karaduman, T. Çorlu, B. Akata, M. A. Yıldırım, A. Ateş and S. Acar, *J. Mater. Sci.: Mater. Electron.*, 2018, **29**, 1356–1368.
240 D. C. Pugh, E. J. Newton, A. J. T. Naik, S. M. V. Hailes and I. P. Parkin, *J. Mater. Chem. A*, 2014, **2**, 4758–4764.
241 P. Tarttelin Hernández, S. M. V. Hailes and I. P. Parkin, *Sens. Actuators, B*, 2017, **242**, 1281–1295.
242 A. T. Güntner, S. Abegg, K. Wegner and S. E. Pratsinis, *Sens. Actuators, B*, 2018, **257**, 916–923.
243 E. G. Derouane and S. M. Roberts, *Microporous and mesoporous solid catalysts*, John Wiley & Sons, 2006.
244 U. P. Tran, K. K. Le and N. T. Phan, *ACS Catal.*, 2011, **1**, 120–127.
245 S. K. Brown, M. R. Sim, M. J. Abramson and C. N. Gray, *Indoor Air*, 1994, **4**, 123–134.
246 Z. Wang, C. Hou, Q. De, F. Gu and D. Han, *ACS Sens.*, 2018, **3**, 468–475.
247 Y. Sun, H. Yang, Z. Zhao, K. Suematsu, P. Li, Z. Yu, W. Zhang and J. Hu, *Sens. Actuators, B*, 2020, **318**, 128222.
248 F. Krumeich, S. Abegg and A. T. Güntner, *Z. Anorg. Allg. Chem.*, 2020, **646**, 412–418.
249 A. Y. Volkov, *Platinum Met. Rev.*, 2004, **48**, 3–11.
250 M. A. Portnoff, R. Grace, A. M. Guzman, P. D. Runco and L. N. Yannopoulos, *Sens. Actuators, B*, 1991, **5**, 231–235.
251 V. Bessonneau and O. Thomas, *Int. J. Environ. Res. Public Health*, 2012, **9**, 868–879.
252 L. F. Liotta, *Appl. Catal., B*, 2010, **100**, 403–412.
253 R. Kikuchi, S. Maeda, K. Sasaki, S. Wennerström and K. Eguchi, *Appl. Catal., A*, 2002, **232**, 23–28.
254 Z. Abbasi, M. Haghighi, E. Fatehifar and S. Saedy, *J. Hazard. Mater.*, 2011, **186**, 1445–1454.
255 R. Strobel, A. Baiker and S. E. Pratsinis, *Adv. Powder Technol.*, 2006, **17**, 457–480.
256 L. Machala, R. Zboril and A. Gedanken, *J. Phys. Chem. B*, 2007, **111**, 4003–4018.
257 J. C. Védrine, *Catalysts*, 2017, **7**, 314.
258 M. S. Kamal, S. A. Razzak and M. M. Hossain, *Atmos. Environ.*, 2016, **140**, 117–134.
259 J. W. Maina, C. Pozo-Gonzalo, L. Kong, J. Schütz, M. Hill and L. F. Dumée, *Mater. Horiz.*, 2017, **4**, 345.
260 M. A. Sidheswaran, H. Destaillats, D. P. Sullivan, J. Larsen and W. J. Fisk, *Appl. Catal., B*, 2011, **107**, 34–41.
261 H. Huang, Y. Xu, Q. Feng and D. Y. C. Leung, *Catal. Sci. Technol.*, 2015, **5**, 2649–2669.
262 H. A. Benesi, *J. Catal.*, 1967, **8**, 368–374.
263 R. K. Sharma, B. Zhou, S. Tong and K. T. Chuang, *Ind. Eng. Chem. Res.*, 1995, **34**, 4310–4317.
264 R. J. Farrauto, M. Deeba and S. Alerasool, *Nat. Catal.*, 2021, **2**, 603–613.
265 Z. Li, D. Wang, Y. Wu and Y. Li, *Natl. Sci. Rev.*, 2018, **5**, 673–689.
266 M. Phillips, *Anal. Biochem.*, 1997, **247**, 272–278.
267 A. G. Panov and J. J. Fripiat, *J. Catal.*, 1998, **178**, 188–197.
268 M. Frankel, G. Bekö, M. Timm, S. Gustavsen, E. W. Hansen and A. M. Madsen, *Appl. Environ. Microbiol.*, 2012, **78**, 8289–8297.
269 J. A. Moulijn, O. W. N. M. van Leeuwen and R. A. Santen, *Stud. Surf. Sci. Catal.*, 1993, **79**, 69–86.
270 F. A. Smith, S. Elliott, D. R. Blake and F. S. Rowland, *Environ. Sci. Policy*, 2002, **5**, 449–461.
271 T. G. Leighton and P. R. White, *Proc. R. Soc. A*, 2012, **468**, 485–510.
272 S. Basu and P. K. Basu, *J. Sens.*, 2009, **2009**, 861968.
273 B. Vanderstraeten, J. Berghmans, D. Tuerlinckx, B. Smit, E. Van't Oost and S. Vliegen, *J. Hazard. Mater.*, 1997, **56**, 237–246.
274 S. Prasad, L. Zhao and J. Gomes, *Epidemiology*, 2011, **22**, 251.
275 T. Sahm, W. Rong, N. Bârsan, L. Mädler, S. K. Friedlander and U. Weimar, *J. Mater. Res.*, 2007, **22**, 850–857.
276 P. Reimann and A. Schütze, *Sens. Rev.*, 2012, **32**, 47–58.
277 V. Weli and J. O. Adegoke, *J. Pollut. Control*, 2016, **4**, 1000171.
278 A. Cabot, J. Arbiol, A. Cornet, J. R. Morante, F. Chen and M. Liu, *Thin Solid Films*, 2003, **436**, 64–69.
279 S. Ghosh, C. Roychaudhuri, R. Bhattacharya, H. Saha and N. Mukherjee, *ACS Appl. Mater. Interfaces*, 2014, **6**, 3879–3887.
280 S. Ghosh, R. Bhattacharyya, H. Saha, C. R. Chaudhuri and N. Mukherjee, *Phys. Chem. Chem. Phys.*, 2015, **17**, 27777–27788.
281 N. Ikoma, M. Takeya and N. Satoshi, *Combustible gas sensor and method for detecting deterioration of catalyst*, EP0751390A3, 1995.
282 S. Jansat, K. Pelzer, J. Garcia-Anton, R. Raucoules, K. Philippot, A. Maisonnat, B. Chaudret, Y. Guari, A. Mehdi, C. Reye and R. J. R. Corriu, *Adv. Funct. Mater.*, 2007, **17**, 3339–3347.
283 T. Sahm, W. Rong, N. Bârsan, L. Mädler and U. Weimar, *Sens. Actuators, B*, 2007, **127**, 63–68.
284 T. Suzuki, K. Kunihara, M. Kobayashi, S. Tabata, K. Higaki and H. Ohnishi, *Sens. Actuators, B*, 2005, **109**, 185–189.
285 K. Sahner, R. Moos, M. Matam, J. J. Tunney and M. Post, *Sens. Actuators, B*, 2005, **108**, 102–112.
286 M. Fleischer, S. Kornely, T. Weh, J. Frank and H. Meixner, *Sens. Actuators, B*, 2000, **69**, 205–210.
287 G. G. Mandayo, E. Castaño, F. J. Gracia, A. Cirera, A. Cornet and J. R. Morante, *Sens. Actuators, B*, 2002, **87**, 88–94.
288 F. S. Fateminia, Y. Mortazavi and A. A. Khodadadi, *Mater. Sci. Semicond. Process.*, 2019, **90**, 182–189.
289 B. A. Tichenor and M. A. Palazzolo, *Environ. Prog.*, 1987, **6**, 172–176.
290 H. H. Kung, M. Kung and C. Costello, *J. Catal.*, 2003, **216**, 425–432.
291 S. N. Oliaee, A. Khodadadi, Y. Mortazavi and S. Alipour, *Sens. Actuators, B*, 2010, **147**, 400–405.
292 J. Jońca, J. Harmel, L. Joanny, A. Ryzhikov, M. L. Kahn, P. Fau, B. Chaudret and K. Fajerwerg, *Sens. Actuators, B*, 2017, **249**, 357–363.

293 J. Vuković, D. Modun, D. Marković and D. Sutlović, *J. Subst. Abuse Alcohol.*, 2015, **3**, 1029.
294 A. T. Güntner, I. C. Weber and S. E. Pratsinis, *ACS Sens.*, 2020, **5**, 1058–1067.
295 M. P. Kalapos, *Biochim. Biophys. Acta*, 2003, **1621**, 122–139.
296 N. C. Jeong, J. S. Lee, E. L. Tae, Y. J. Lee and K. B. Yoon, *Angew. Chem., Int. Ed.*, 2008, **47**, 10128–10132.
297 T. Mallat and A. Baiker, *Chem. Rev.*, 2004, **104**, 3037–3058.
298 J. Llorca, N. Homs and P. Ramirez de la Piscina, *J. Catal.*, 2004, **227**, 556–560.
299 A. Mirzaei, J.-H. Kim, H. W. Kim and S. S. Kim, *J. Mater. Chem. C*, 2018, **6**, 4342–4370.
300 S.-Y. Jeong, J.-W. Yoon, T.-H. Kim, H.-M. Jeong, C.-S. Lee, Y. Chan Kang and J.-H. Lee, *J. Mater. Chem. A*, 2017, **5**, 1446–1454.
301 J. Hubálek, K. Malysz, J. Prášek, X. Vilanova, P. Ivanov, E. Llobet, J. Brezmes, X. Correig and Z. Svěrák, *Sens. Actuators, B*, 2004, **101**, 277–283.
302 P. Clément, S. Korom, C. Struzzi, E. J. Parra, C. Bittencourt, P. Ballester and E. Llobet, *Adv. Funct. Mater.*, 2015, **25**, 4011–4020.
303 H.-M. Jeong, S.-Y. Jeong, J.-H. Kim, B.-Y. Kim, J.-S. Kim, F. Abdel-Hady, A. A. Wazzan, H. A. Al-Turaif, H. W. Jang and J.-H. Lee, *ACS Appl. Mater. Interfaces*, 2017, **9**, 41397–41404.
304 L. Cao, Z. Gao, S. L. Suib, T. N. Obee, S. O. Hay and J. D. Freihaut, *J. Catal.*, 2000, **196**, 253–261.
305 Y. Zeng, Z. Hua, X. Tian, X. Li, Z. Qiu, C. Zhang, M. Wang and E.-P. Li, *Sens. Actuators, B*, 2018, **273**, 1291–1299.
306 M. H. Saberi, Y. Mortazavi and A. A. Khodadadi, *Sens. Actuators, B*, 2015, **206**, 617–623.
307 G. Korotcenkov, B. K. Cho, V. Brinzari, L. B. Gulina and V. P. Tolstoy, *Ferroelectrics*, 2014, **459**, 46–51.
308 M. Frietsch, F. Zudock, J. Goschnick and M. Bruns, *Sens. Actuators, B*, 2000, **65**, 379–381.
309 D. P. Mann, K. F. E. Pratt, T. Paraskeva, I. P. Parkin and D. E. Williams, *IEEE Sens. J.*, 2007, **7**, 551–556.
310 J. Wöllenstein, H. Böttner, M. Jaegle, W. J. Becker and E. Wagner, *Sens. Actuators, B*, 2000, **70**, 196–202.
311 K. Sahner, D. Schönauer, P. Kuchinke and R. Moos, *Sens. Actuators, B*, 2008, **133**, 502–508.
312 S.-Y. Jeong, Y. K. Moon, T.-H. Kim, S.-W. Park, K. B. Kim, Y. C. Kang and J.-H. Lee, *Adv. Sci.*, 2020, **7**, 1903093.
313 V. Paul, R. Pandey and G. C. Srivastava, *J. Food Sci. Technol.*, 2012, **49**, 1–21.
314 H. P. Hofmann, *Catal. Rev.: Sci. Eng.*, 1978, **17**, 71–117.
315 A. T. Güntner, N. A. Sievi, S. J. Theodore, T. Gulich, M. Kohler and S. E. Pratsinis, *Anal. Chem.*, 2017, **89**, 10578–10584.
316 A. T. Güntner, J. F. Kompalla, H. Landis, S. J. Theodore, B. Geidl, N. A. Sievi, M. Kohler, S. E. Pratsinis and P. A. Gerber, *Sensors*, 2018, **18**, 3655.
317 A. T. Güntner, N. J. Pineau, P. Mochalski, H. Wiesenhofer, A. Agapiou, C. A. Mayhew and S. E. Pratsinis, *Anal. Chem.*, 2018, **90**, 4940–4945.
318 R. Yoo, A. T. Güntner, Y. Park, H. J. Rim, H. S. Lee and W. Lee, *Sens. Actuators, B*, 2019, **283**, 107–115.
319 P. Mochalski, V. Ruzsanyi, H. Wiesenhofer and C. A. Mayhew, *J. Breath Res.*, 2018, **12**, 027107.
320 K. Tadesse, D. Smith and M. A. Eastwod, *Q. J. Exp. Physiol. Cogn. Med. Sci.*, 1980, **65**, 85–97.
321 M. Righettoni, A. Ragnoni, A. T. Güntner, C. Loccioni, S. E. Pratsinis and T. H. Risby, *J. Breath Res.*, 2015, **9**, 047101.
322 A. Lewis and P. Edwards, *Nature*, 2016, **535**, 29–31.
323 F. Bindler, E. Voges and P. Laugel, *Food Addit. Contam.*, 1988, **5**, 343–351.
324 J. A. Kraut, *Am. J. Kidney Dis.*, 2016, **68**, 161–167.
325 C. Wambua-Soi, Iran: Over 700 dead after drinking alcohol to cure coronavirus, https://www.aljazeera.com/news/2020/04/iran-700-dead-drinking-alcohol-cure-coronavirus-200427163529629.html, Al-Jazeera, 2020/04/27.
326 M. Fazio, 3 Die in New Mexico After Drinking Hand Sanitizer, Officials Say, https://www.nytimes.com/2020/06/26/us/3-dead-drinking-hand-sanitizer.html, The New York Times, 2020/06/26.
327 D. M. Ruszkiewicz, D. Sanders, R. O'Brien, F. Hempel, M. J. Reed, A. C. Riepe, K. Bailie, E. Brodrick, K. Darnley, R. Ellerkmann, O. Mueller, A. Skarysz, M. Truss, T. Wortelmann, S. Yordanov, C. L. P. Thomas, B. Schaaf and M. Eddleston, *EClinicalMedicine*, 2020, https://doi.org/10.1016/j.eclinm.2020.100609.
328 A. C. Skinner, S. N. Ravanbakht, J. A. Skelton, E. M. Perrin and S. C. Armstrong, *Pediatrics*, 2018, **141**(3), e20173459.
329 S. Kaskel, *The Chemistry of Metal–Organic Frameworks*, Wiley, 2016, pp. 271–307.
330 M. L. Terranova, S. Orlanducci and M. Rossi, *Carbon nanomaterials for gas adsorption*, CRC Press, 2012.
331 D. W. Breck, *Zeolite molecular sieves: structure, chemistry and use*, Krieger, 1984.
332 M. Van-Leeuwen, *Fluid Phase Equilib.*, 1994, **99**, 1–18.
333 M. Arruebo, J. L. Falconer and R. D. Noble, *J. Membr. Sci.*, 2006, **269**, 171–176.

